**Supplementary Information**

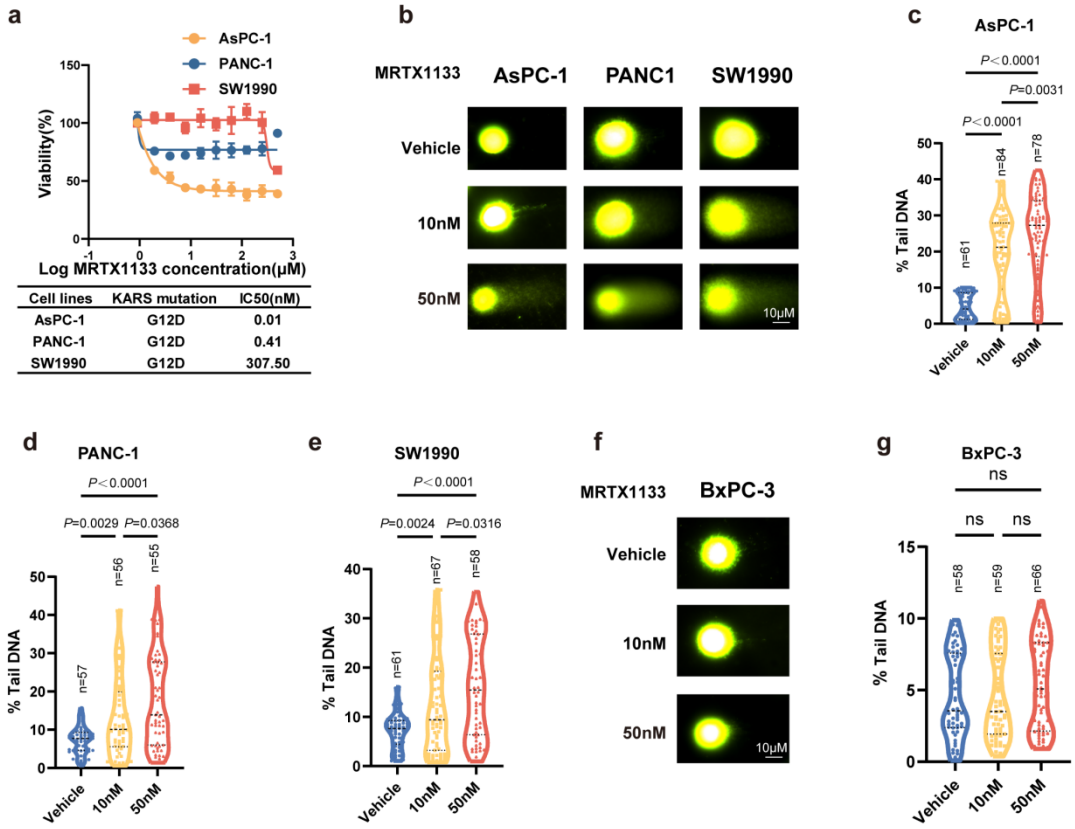


| Cell lines | KARS mutation | IC50(nM) |
|---|---|---|
| AsPC-1 | G12D | 0.01 |
| PANC-1 | G12D | 0.41 |
| SW1990 | G12D | 307.50 |

**Supplementary figure 1. MRTX1133 induces DNA damage specifically in KRAS$^{G12D}$ mutant pancreatic cancer cells.**

**a** Cell viability curves for KRAS$^{G12D}$ mutant cell lines (AsPC-1, PANC-1, SW1990) following a 48-hour treatment with MRTX1133. The table below lists the specific KRAS mutation and calculated $IC_{50}$ value for each cell line. Data are presented as mean ± SEM from three biological replicates.

**b-e** DNA damage response of KRAS$^{G12D}$ cell lines to MRTX1133. (**b**) Representative images from comet assays performed on three KRAS$^{G12D}$ mutant pancreatic cancer cell lines (AsPC-1, PANC-1, and SW1990) and BxPC-3 cells following treatment with MRTX1133. Comets indicate the extent of DNA strand breaks. (**c-e**) Quantification of DNA damage using tail DNA percentage as the metric. Data are presented as violin plots. The thick dashed line represents the median, and the thin dashed lines represent the quartiles (25th and 75th percentiles). Each dot represents an

individual cell. The sample size (n) for each group is indicated above the violin. Statistical significance was determined by one-way ANOVA followed by multiple comparisons test.

**f-g** DNA damage response of $KRAS^{WT}$ cell line to MRTX1133. BxPC-3 $KRAS^{WT}$ was treated with MRTX1133 (50nM) for 24h. Representative micrographs (**f**) of comet assay of BxPC-3 at 4h post irradiation. Comets indicate the extent of DNA strand breaks. (**g**) Quantification of DNA damage using tail DNA percentage as the metric. Data are presented as violin plots. The thick dashed line represents the median, and the thin dashed lines represent the quartiles (25th and 75th percentiles). Each dot represents an individual cell. The sample size (n) for each group is indicated above the violin. Statistical significance was determined by one-way ANOVA followed by multiple comparisons test.

Ns, no significant. Source data are provided as a Source Data file.

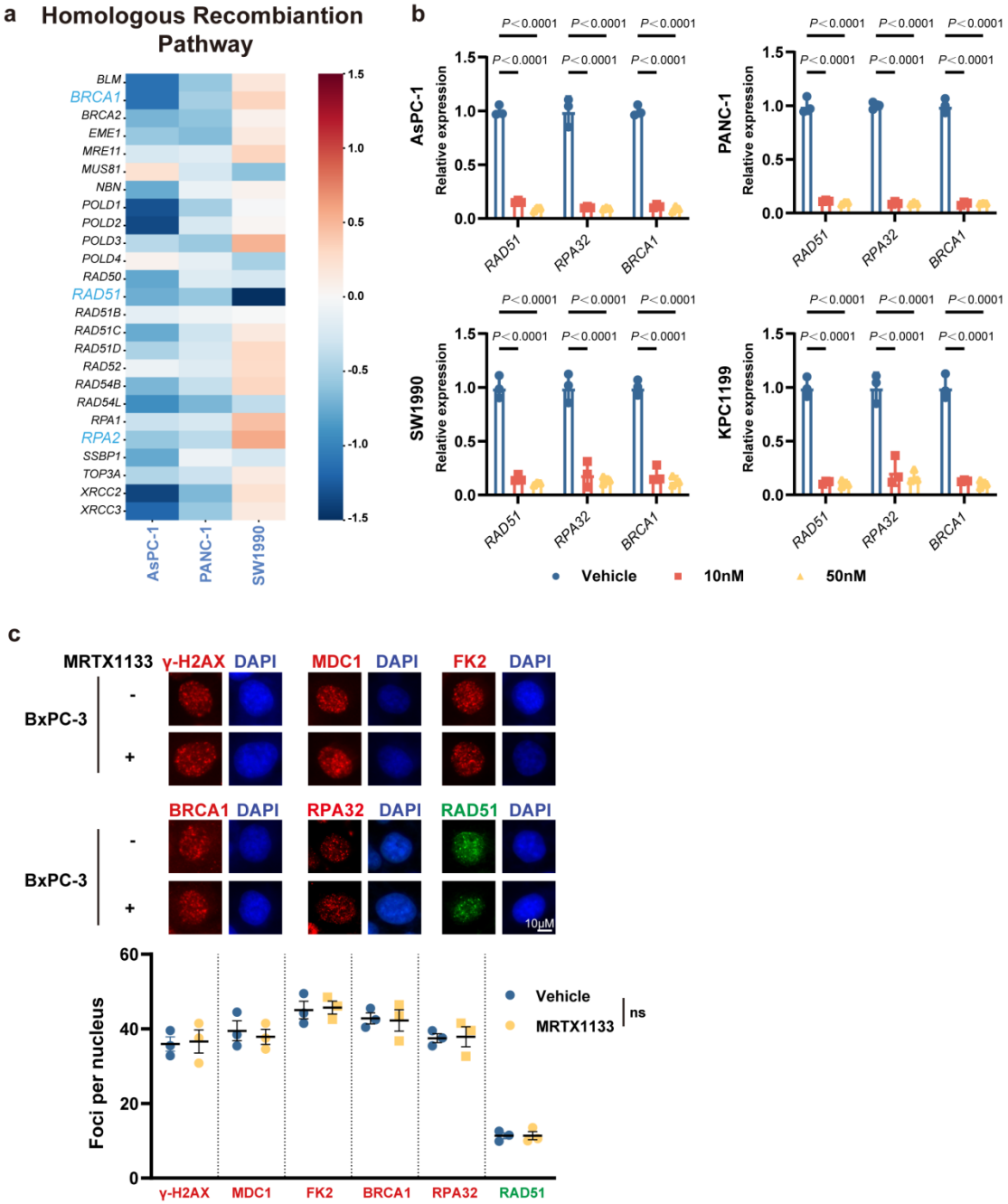


**Supplementary figure 2. The alternative situation of HR Deficiency in other KRAS mutants response to indicated inhibitors.**

**a** Heatmap plot of HR-related genes. RNA-seq analysis of KRAS $^{G12D}$ cells treated with 50nM MRTX1133(AsPC-1, PANC-1 and SW1990) for 24h. Heatmap depicting the differential expression of the indicated genes that are involved in HR signaling.

**b** Relative mRNA expression of key HR genes (*RAD51, RPA32, BRCA1*) in four $KRAS^{G12D}$ mutant cell lines treated with MRTX1133 (10 nM or 50 nM) for 24 hours. Data were determined by RT-qPCR and are presented as mean ± SEM from three biological replicates, with individual technical replicates shown as dots. Statistical significance was determined by one-way ANOVA.

**c** Immunofluorescence assay for DNA damage marker in cell lines with $KRAS^{WT}$. Representative micrographs and quantification data for γ-H2AX, MDC1, FK2, BRCA1, RPA32 and RAD51 foci formation in the $KRAS^{WT}$ BxPC-3 cell with and without MRTX1133 treatment (50nM). Data are presented as mean ± SEM of n=3 biologically independent experiments. Statistical significance was determined by the two-tailed unpaired t-test. The scale bar indicates 10 μm.

Ns, no significant. Source data are provided as a Source Data file.

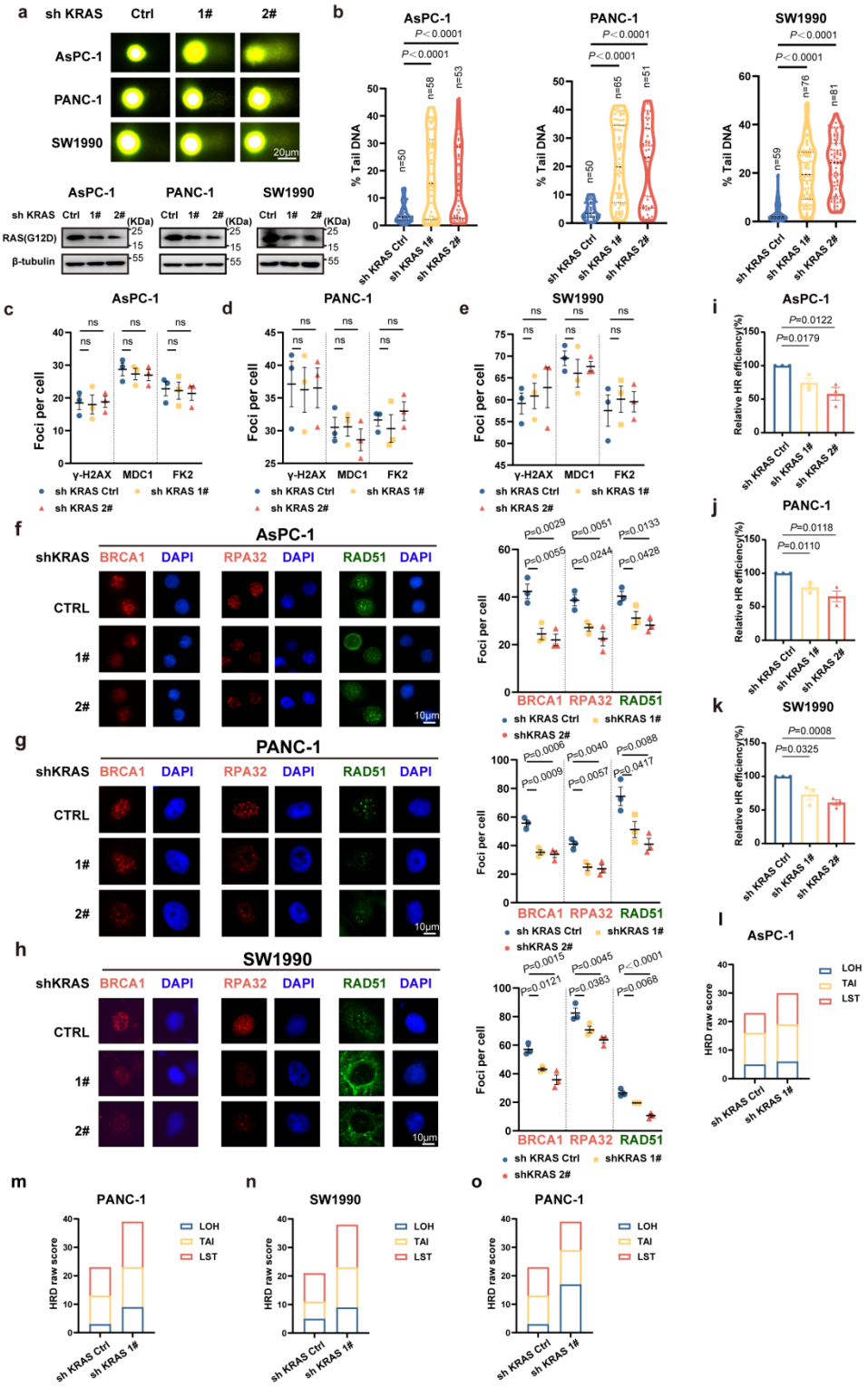


**Supplementary figure 3. KRAS$^{G12D}$ specific knockdown induces HR deficiency**

**a** Comet assay analysis of DNA damage in KRAS-knockdown cells. Representative images from comet assays performed on three KRAS$^{G12D}$ mutant pancreatic cancer

cell lines (AsPC-1, PANC-1, and SW1990) after transduction with two different shRNAs targeting KRAS (1#, 2#) compared to a non-targeting control (Ctrl). Western blot confirming the successful knockdown of KRAS protein by the shRNAs. β-tubulin serves as a loading control.

**b** Quantification of DNA damage (**a**) using tail DNA percentage as the metric. Data are presented as violin plots. Sample sizes (n) for each group are indicated in the figure.

**c-e** Quantification of early DNA damage response foci ( γ -H2AX, MDC1, FK2) in AsPC-1 (**c**), PANC-1 (**d**), and SW1990 (**e**) cells following KRAS knockdown. Data are presented as mean ± SEM of n=3 biologically independent experiments. Statistical significance was determined by one-way ANOVA.

**f-h** Immunofluorescence analysis of key HR protein foci in AsPC-1 (**f**), PANC-1 (**g**), and SW1990 (**h**) cells after KRAS knockdown. For each cell line, representative images (left) and quantification (right) of BRCA1, RPA32, and RAD51 foci are shown. Data are presented as mean ± SEM of n=3 biologically independent experiments. Statistical significance was determined by one-way ANOVA.

**i-k** HR efficiency in KRAS-knockdown cells using the DR-GFP reporter system. Measurement of homologous recombination (HR) efficiency in AsPC-1 (**i**), PANC-1 (**j**), and SW1990 (**k**) cell lines following KRAS knockdown, assessed via the DR-GFP reporter system and flow cytometry analysis. Data are presented as mean ± SEM of n=3 biologically independent experiments. Statistical significance was determined by one-way ANOVA.

**l-o** HRD scores in pancreatic cancer cell lines with different KRAS expression. (**l-n**) Bar graphs depicting HRD scores, including loss of heterozygosity (LOH), telomeric allelic imbalance (TAI), and large-scale state transitions (LST), in control (Ctrl) and KRAS-knockdown (1#) conditions for AsPC-1 (**l**), PANC-1 (**m**), and SW1990 (**n**)

cell lines. (**o**) As a positive control, BRCA1 knockdown (shBRCA1) in PANC-1 cells markedly increased HRD scores.

Ns, no significant. Source data are provided as a Source Data file.

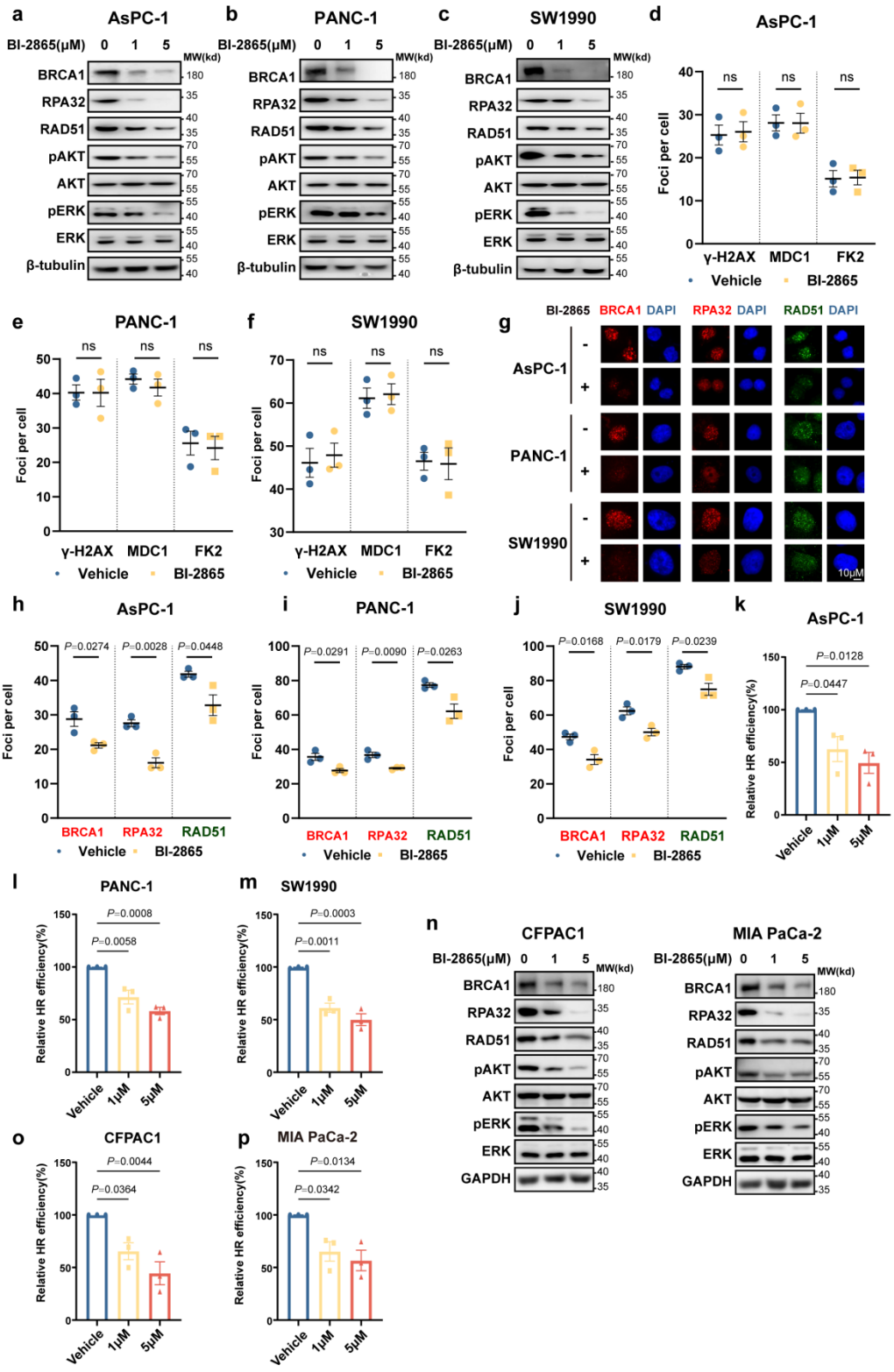


**Supplementary figure 4. The pan-RAS inhibitor BI-2865 induces Homologous Recombination Deficiency (HRD) in KRAS mutant pancreatic cancer cells.**

**a-c** Western blot analysis of BRCA1, RPA32, RAD51, total ERK, total AKT, phospho-ERK, and phospho-AKT protein levels in $KRAS^{G12D}$ pancreatic cancer cell lines AsPC-1(**a**), PANC-1(**b**) and SW1990(**c**) treated with vehicle (DMSO) or BI-2865 at the indicated concentrations for 24 hours. Cell lysates were collected for immunoblotting.

**d-f** Immunofluorescence detection of DNA damage marker foci in $KRAS^{G12D}$ pancreatic cancer cells treated with BI-2865. Quantification data for γ-H2AX, MDC1 and FK2 foci formation in the indicated cell lines AsPC-1(**d**), PANC-1(**e**) and SW1990(**f**) with and without BI-2865 treatment (5 μM) at 1 h after 2Gy X-ray irradiation treatment (γ-H2AX, MDC1 and FK2). Data are presented as mean ± SEM of n=3 biologically independent experiments. Statistical significance was determined by unpaired, two-tailed Student's t-test.

**g-j** Immunofluorescence detection of HR marker foci in $KRAS^{G12D}$ pancreatic cancer cells treated with BI-2865. Representative micrographs (**g**) and quantification data for BRCA1, RPA32 and RAD51 foci formation (**h-j**) in the indicated cell lines with and without BI-2865 treatment (5 μM). Data are presented as mean ± SEM of n=3 biologically independent experiments. Statistical significance was determined by unpaired, two-tailed Student's t-test. The scale bar indicates 10 μm.

**k-m** Inhibition of $KRAS^{G12D}$ by BI-2865 decreased HR repair efficiency in $KRAS^{G12D}$ pancreatic cancer cells. AsPC-1(**k**), PANC-1(**l**), and SW1990(**m**) were treated with BI-2865(1 μM，5 μM). Data are presented as mean ± SEM of n=3 biologically independent experiments. Statistical significance was determined by one-way ANOVA tests.

**n** Western blot analysis of BRCA1, RPA32, RAD51, total ERK, total AKT, phosphor-ERK and phosphor-AKT in CFPAC1(G12V) and MIA PaCa-2(G12C) cells treated with vehicle (DMSO), BI-2865 at indicated concentrations for 24h.

**o-p** Inhibition by BI-2865 decreased HR repair efficiency in non-KRAS$^{G12D}$ pancreatic cancer cells. CFPAC1(G12V) and MIA PaCa-2(G12C) cell lines were treated with BI-2865(1 μ M, 5 μ M). Efficiency was measured using DR-GFP reporter assay system. Data are presented as mean ± SEM of n=3 biologically independent experiments. Statistical significance was determined by one-way ANOVA tests.

Ns, not significant. Source data are provided as a Source Data file.

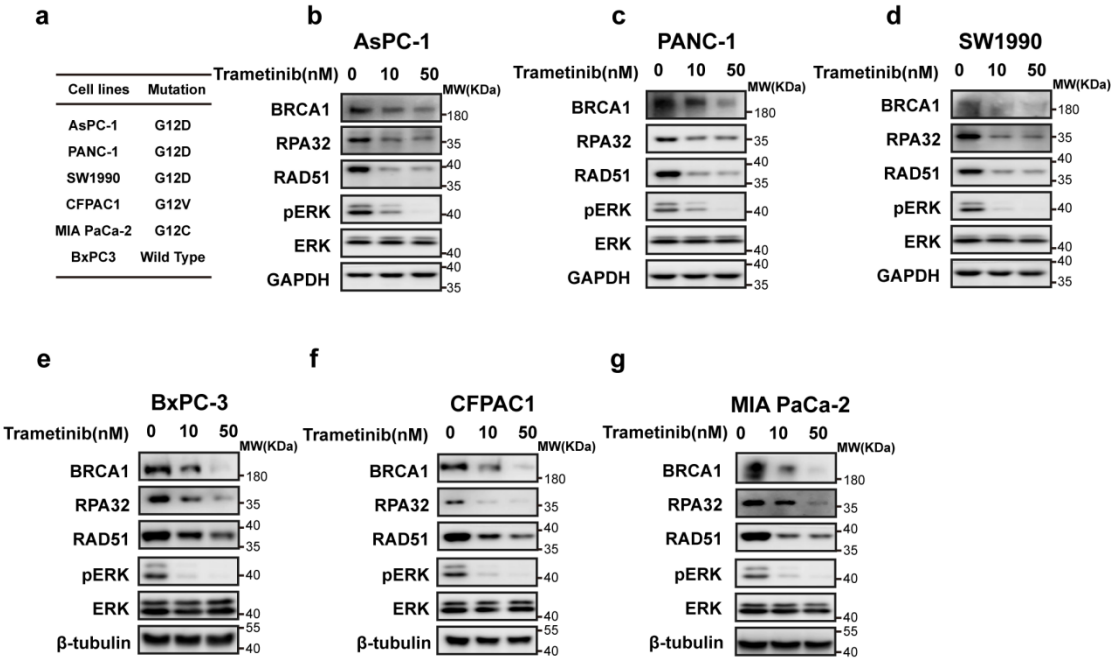


**Supplementary figure 5. The regulation of HR Deficiency in PDAC cell lines to MEK inhibitor.**

**a** Mutation status of KRAS of indicated PDAC cell lines.

**b-g** Western blot analysis of BRCA1, RPA32, RAD51 and phosphor-ERK in pancreatic cell lines treated with vehicle (DMSO), Trametinib at indicated concentrations for 24h. Cell lysate were collected for immunoblotting for BRCA1, RPA32, RAD51, total ERK, and phosphor-ERK. GAPDH and β-tubulin served as the indicated loading control. Experiments were repeated three times independently with similar results.

Source data are provided as a Source Data file.

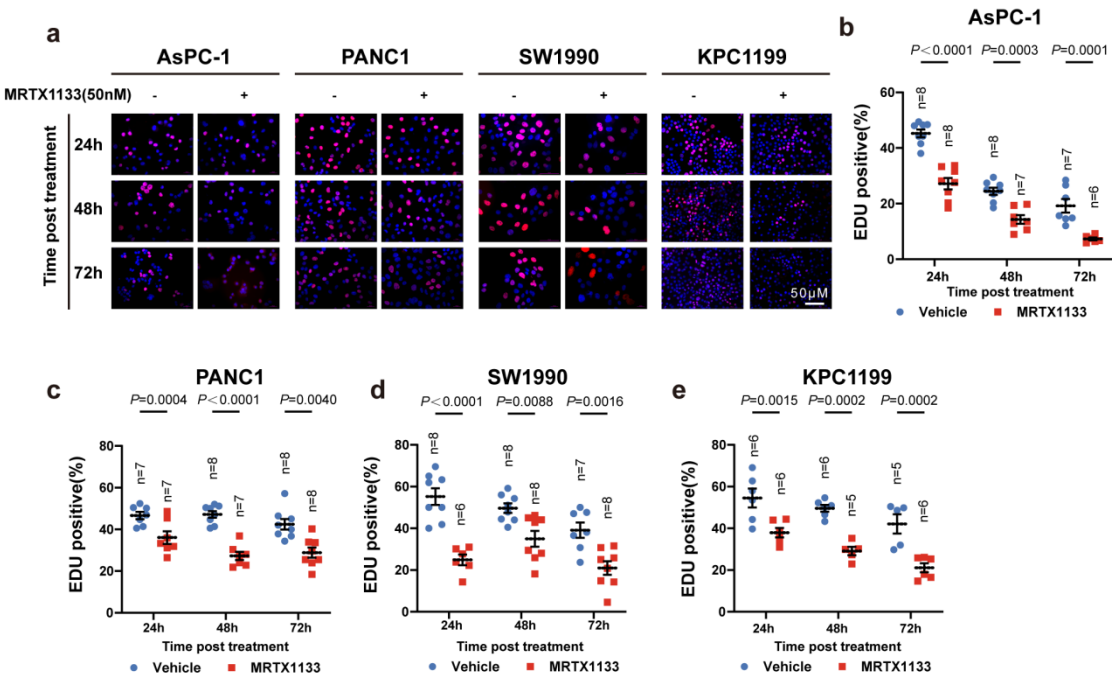


**Supplementary figure 6. MRTX1133 influences cell cycle of KRAS$^{G12D}$ cell lines**

**a** G1/S phase staining in MRTX1133-treated cell lines. Representative images of EdU (5-ethynyl-2'-deoxyuridine) staining for G1/S phase detection in pancreatic cancer cell lines (AsPC-1, PANC-1, SW1990 and KPC1199) at 24, 48, and 72 hours following treatment with 50 nM MRTX1133. Scale bar: 50 μm.

**b-e** Quantification of the percentage of EdU-positive cells for AsPC-1 (**b**), PANC-1 (**c**), SW1990 (**d**), and KPC1199 (**e**). Data are presented as the mean ± SEM from one representative experiment. Sample sizes (n) for each group are indicated in the figure. Each individual point representing a biological replicate (100 cells per time point from n≥5 random fields per group).Statistical significance was determined by a two-way ANOVA. The experiment was repeated three times independently with similar results.

Source data are provided as a Source Data file.

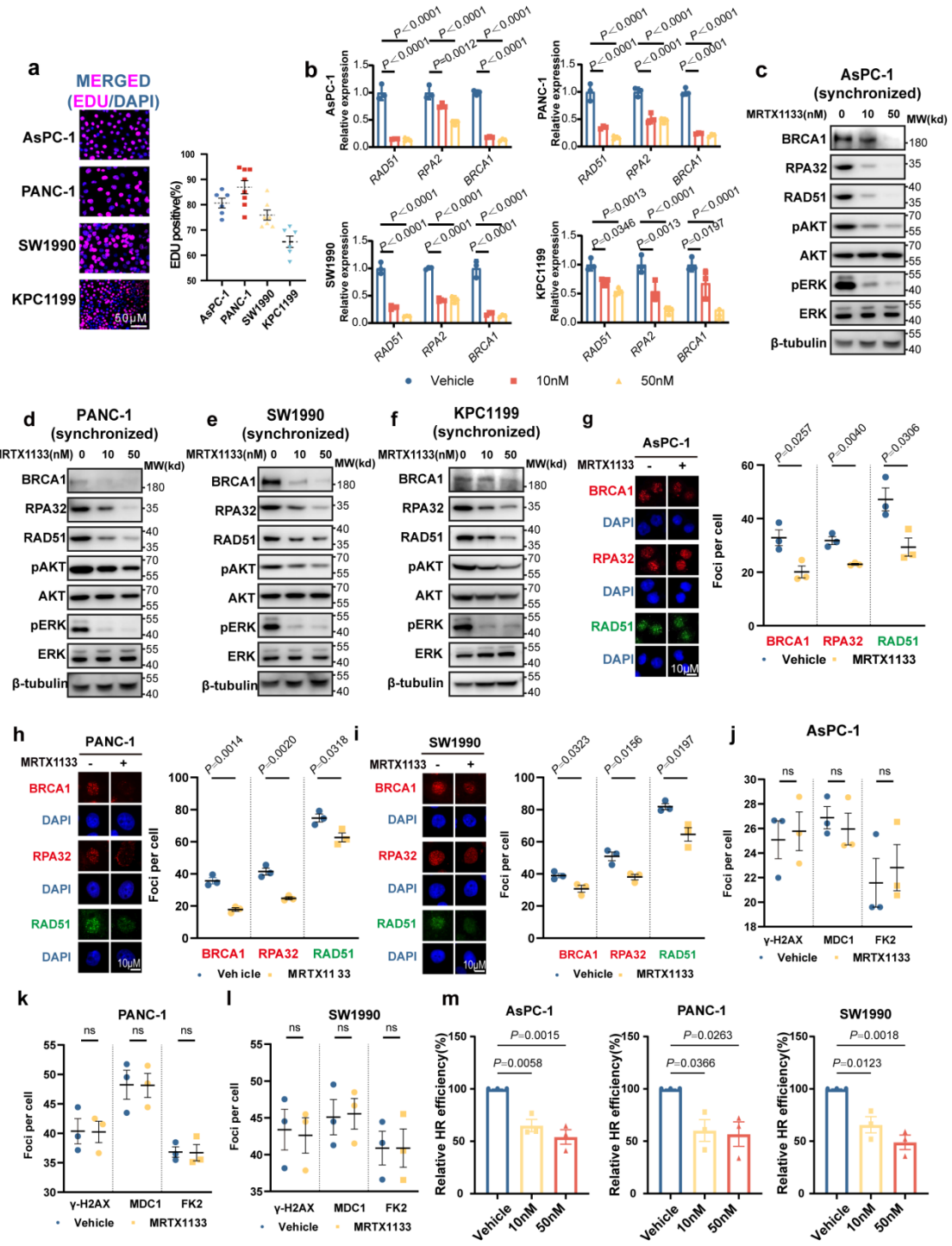


**Supplementary figure 7. The alternative situation of HR Deficiency in synchronized KRAS$^{G12D}$ cell lines to MRTX1133.**

**a** Synchronization efficiency in KRAS$^{G12D}$ mutant cells. Left: Representative EdU staining images of four KRAS$^{G12D}$ cell lines following synchronization. Right: Quantification confirming high rates of EdU-positive cells. Each individual point

representing a biological replicate (100 cells per time point from n⩾5 random fields per group).Bars indicate overall mean ± SEM (n > 100 cells from > 5 fields). Scale bar: 50 μm.

**b** MRTX1133 downregulates homologous recombination-related gene expression in synchronized cells. Relative mRNA levels of *RAD51*, *RPA32*, and *BRCA1* were measured by RT-qPCR after 24 h treatment. Data are presented as bar charts (mean ± SEM) with individual biological replicates. Significance determined by one-way ANOVA.

**c-f** Western blot analysis of BRCA1, RPA32, RAD51, total/phospho-ERK, and total/phospho-AKT levels in synchronized AsPC-1 (**c**), PANC-1 (**d**), SW1990 (**e**), and KPC1199 (**f**) treated with vehicle or MRTX1133 at indicated concentrations for 24 h.

**g-i** Immunofluorescence detection of HR marker foci in synchronized $KRAS^{G12D}$ cell lines. Foci formation was assessed in AsPC-1 (**g**), PANC-1 (**h**), and SW1990 (**i**) treated with MRTX1133 (50 nM). Data are presented as mean ± SEM of n=3 biologically independent experiments. Statistical significance was determined by the two-tailed unpaired t-test. Scale bar: 10 μm. Ns, not significant.

**j-l** Immunofluorescence assay for DNA damage markers in synchronized cell lines. Quantification of γH2AX, MDC1, and FK2 foci in AsPC-1 (**j**), PANC-1 (**k**), and SW1990 (**l**) with or without MRTX1133 (50 nM). Data are presented as mean ± SEM of n=3 biologically independent experiments. Statistical significance was determined by the two-tailed unpaired t-test. Ns, not significant.

**m** MRTX1133 inhibits HR repair efficiency in synchronized pancreatic cancer cells. AsPC-1, PANC-1, and SW1990 were treated with MRTX1133 (10, 50 nM), and efficiency was measured using the DR-GFP reporter assay. Data are presented as mean ± SEM of n=3 biologically independent experiments. Statistical significance was determined by one-way ANOVA.

Source data are provided as a Source Data file.

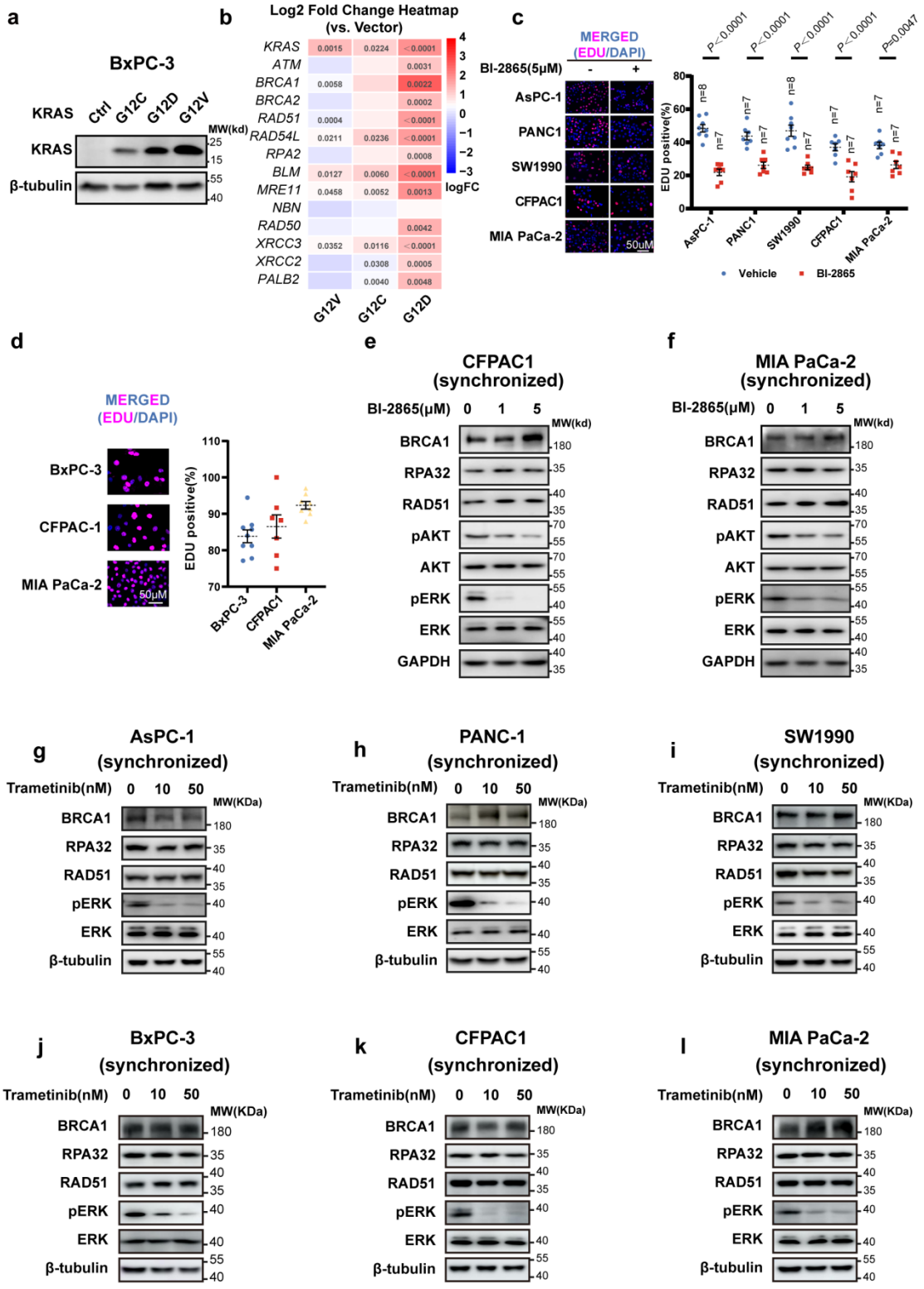


**Supplementary figure 8. The regulation of HR related genes in synchronized non-KRAS$^{G12D}$ cell lines response to BI-2865.**

**a** Western blot confirming the overexpression of various KRAS mutants (G12C, G12D, G12V) in KRAS wild-type BxPC-3 cells. β-tubulin served as a loading control.

**b** Heatmap showing the log2 fold change (logFC) in mRNA expression of HR pathway genes in BxPC-3 cells overexpressing different KRAS mutants compared to a vector control. Data were obtained from RT-qPCR. Red indicates upregulation and blue indicates downregulation. Statistical analysis was performed using two-sided Student's t-tests comparing each mutant group to the control. P-values denoting statistical significance are displayed numerically within the heatmap tiles.

**c** G1/S phase staining in BI-2865 treated cell lines. Representative images of EdU (5-ethynyl-2'-deoxyuridine) staining for G1/S phase detection in pancreatic cancer cell lines at 24 hours following treatment with 5 μM BI-2865. Quantification of EdU-positive cells indicating G1/S phase progression. Data are presented as scatter plots showing mean ± SEM with individual biological replicates. Statistical significance was determined by unpaired, two-tailed Student's t-test for each cell line. Scale bar: 50 μm.

**d** Synchronization efficiency in non-$KRAS^{G12D}$ mutant cells. Representative images of EdU staining in BxPC-3(WT), CFPAC1(G12V) and MIA PaCa-2(G12C) cell lines following synchronization, accompanied by quantification of EdU-positive cell rates using ImageJ software. Data are shown as the mean ± SEM.

**e-f** Western blot analysis of BRCA1, RPA32, RAD51, phosphor-AKT and phosphor-ERK in synchronized non-G12D pancreatic cell lines CFPAC1(**e**) and MIA PaCa-2(**f**) using HU block and treated with vehicle (DMSO), BI-2865 at indicated concentrations for 24h. Cell lysate were collected for immunoblotting for BRCA1, RPA32, RAD51, total ERK, total AKT, phosphor-AKT and phosphor-ERK. GAPDH served as the loading control.

**g-l** Western blot analysis of HR proteins and ERK signaling in synchronized pancreatic cell lines treated with vehicle (DMSO), Trametinib at indicated concentrations for 24h. Cell lysate were collected for immunoblotting for BRCA1, RPA32, RAD51 and phosphor-ERK. β-tubulin served as the indicated loading control.

Source data are provided as a Source Data file.

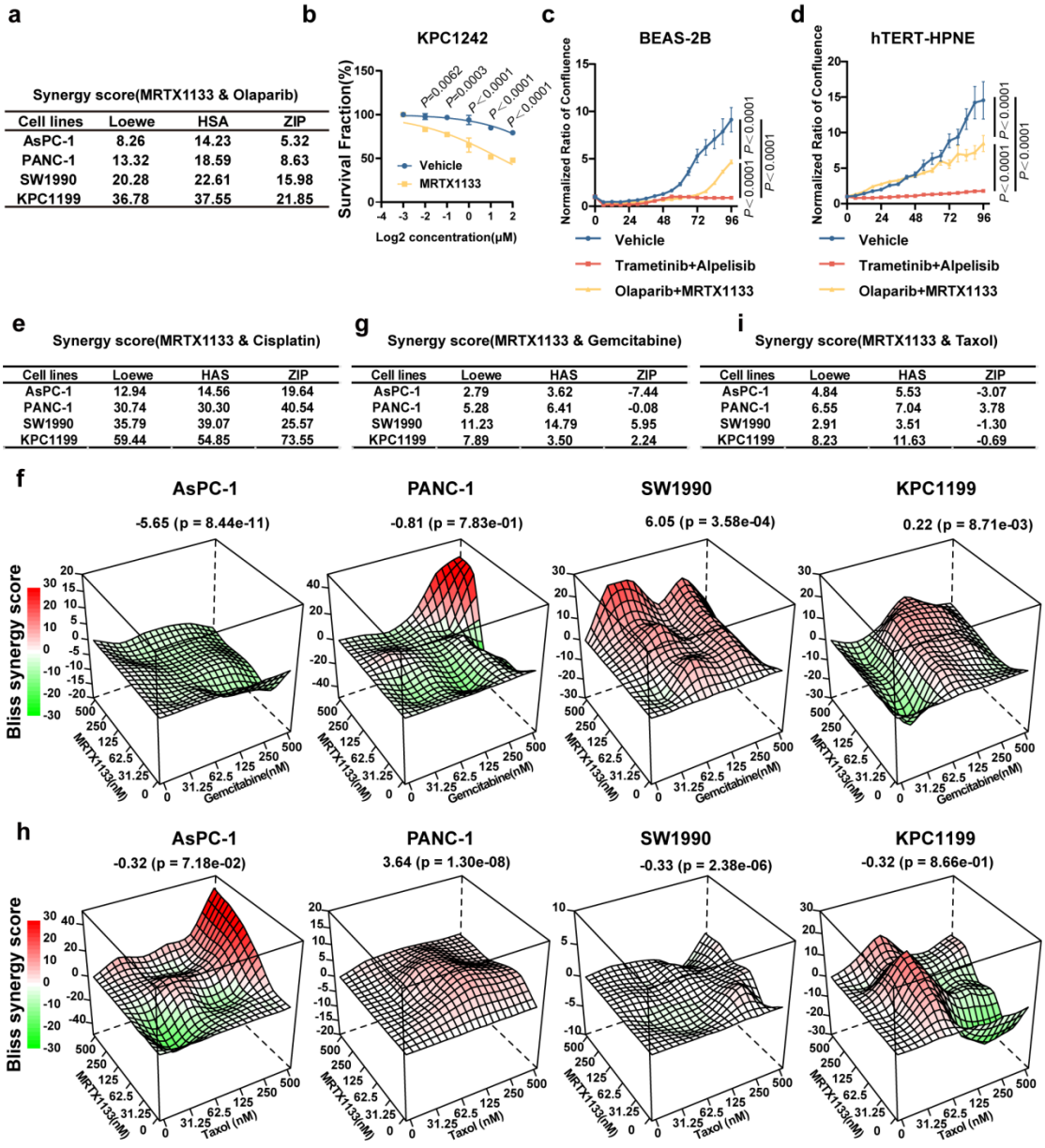


**Supplementary figure 9. PARP inhibitor Olaparib works synergistically with MRTX1133 *in vitro*.**

**a** Table summarizing synergy scores for the combination of MRTX1133 and the PARP inhibitor Olaparib across four KRAS$^{G12D}$ mutant cell lines. Synergy scores were calculated using the Loewe additivity, Highest Single Agent (HSA), and Zero Interaction Potency (ZIP) reference models.

**b** Evaluation of 2-D colony formation in KPC1242 cells in response to Olaparib treatment. Relative colony formation rates were calculated based on colony counts at

Days 10 – 12 post-treatment. Data are presented as mean ± SEM of n=3 biologically independent experiments. Statistical significance for indicated concentrations was determined by two-way ANOVA.

**c-d** The combination of Olaparib and MRTX1133 exhibits minimal toxicity toward non-cancerous cells. Real-time proliferation curves for human bronchial epithelial cells (BEAS-2B, **c**) and pancreatic ductal epithelial cells (hTERT-HPNE, **d**) were monitored over 96 h using the Incucyte live-cell imaging system. Cells were treated with concentrations utilized in cancer cell assays: Vehicle (0.1% DMSO), Trametinib (50 nM) + Alpelisib (50 nM), or Olaparib (100 nM) + MRTX1133 (50 nM). Data are presented as mean ± SEM. Significance was assessed using two-way ANOVA.

**e** Synergy scores for Cisplatin combined with MRTX1133. Scores were analyzed using HSA, Loewe, and ZIP models as listed in the table.

**f** 3D Bliss synergy landscapes for four $KRAS^{G12D}$ cell lines treated with combinations of MRTX1133 and Gemcitabine. Red peaks indicate synergy, while green valleys indicate antagonism. Data represent the mean of three independent biological replicates (n=3). Statistical significance of the synergy score was determined by a one-sample t-test comparing the mean synergy score against a reference value of 0 (two-sided).

**g** Synergy scores for Gemcitabine combined with MRTX1133, analyzed using HSA, Loewe, and ZIP models.

**h** 3D Bliss synergy landscapes for four $KRAS^{G12D}$ cell lines treated with combinations of MRTX1133 and Taxol. Data represent the mean of three independent biological replicates (n=3). Statistical significance of the synergy score was determined by a one-sample t-test comparing the mean synergy score against a reference value of 0 (two-sided).

**i** Synergy scores for Taxol combined with MRTX1133, analyzed using HSA, Loewe, and ZIP models.

Source data are provided as a Source Data file.

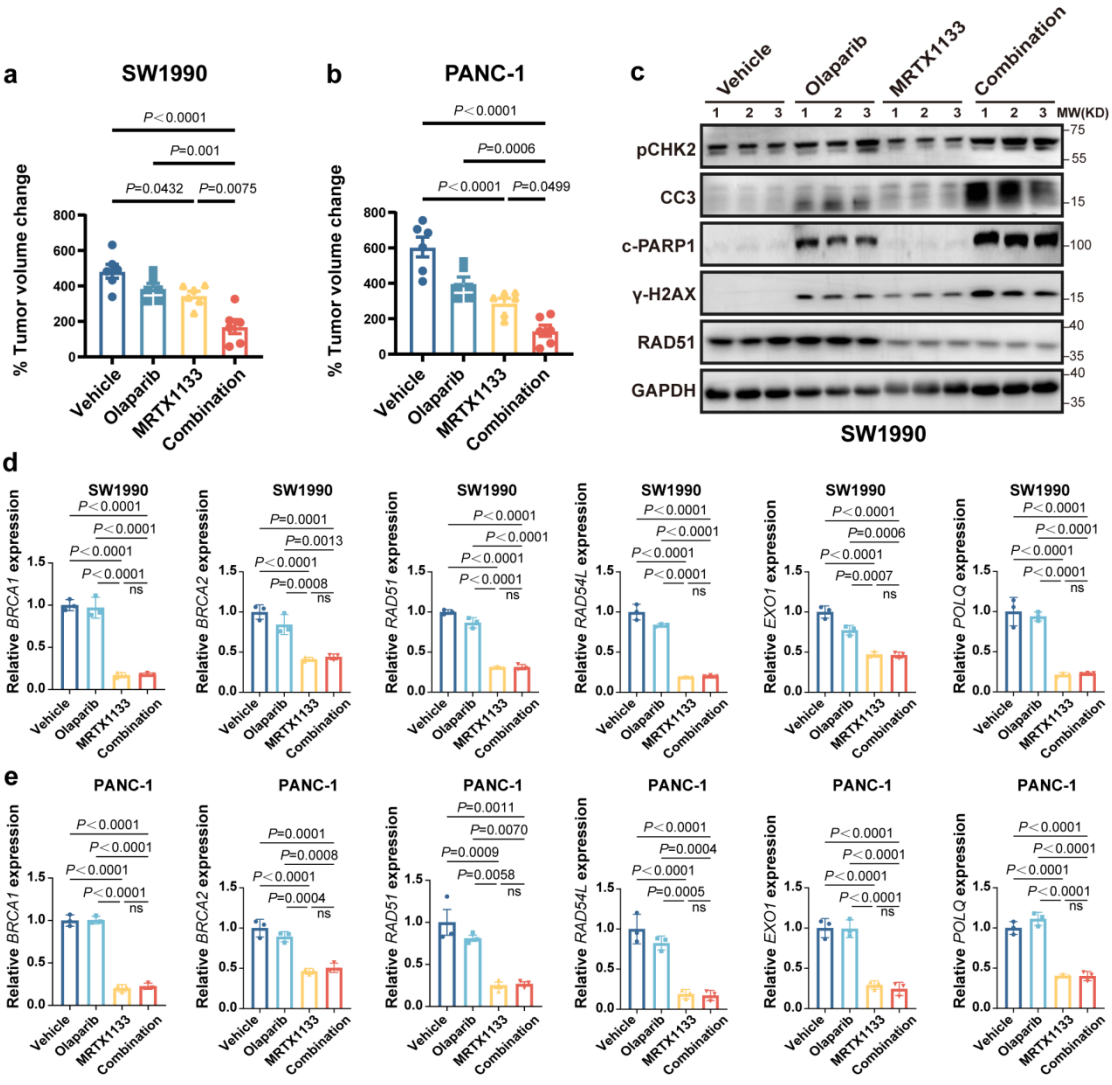


**Supplementary figure 10. Downregulated HR pathway in PDAC cell derived xenograft.**

**a-b** Relative SW1990 (**a**) and PANC-1 (**b**) tumor volume. Tumor volume was measured every day. Bar charts show the endpoint tumor volume change (as a percentage of baseline) in mice bearing SW1990 (**a**) or PANC-1 (**b**) xenografts. Each dot represents an individual mouse (n=6 per group). Data are represented as the Mean ± SEM. Statistical significance was determined by one-way ANOVA.

**c** Western blots showing indicated protein changes in tumor tissues after treatment in SW1990 xenografts. pCHK2: phosphorous-Checkpoint kinase 2; CC3: cleaved-caspase 3; c-PARP1: cleaved PARP1 (n=3 representative mice per group).

**d-e** RNA level of HR-related genes among all subgroups in SW1990(**d**) and PANC-1(**e**) derived xenograft tumor tissue. Transcriptional diminution of the HR related genes in MRTX1133-involved therapy was confirmed. 3 animals per group. Data are represented as the Mean ± SEM. Statistical significance was determined by one-way ANOVA. Ns, no significant. Source data are provided as a Source Data file.

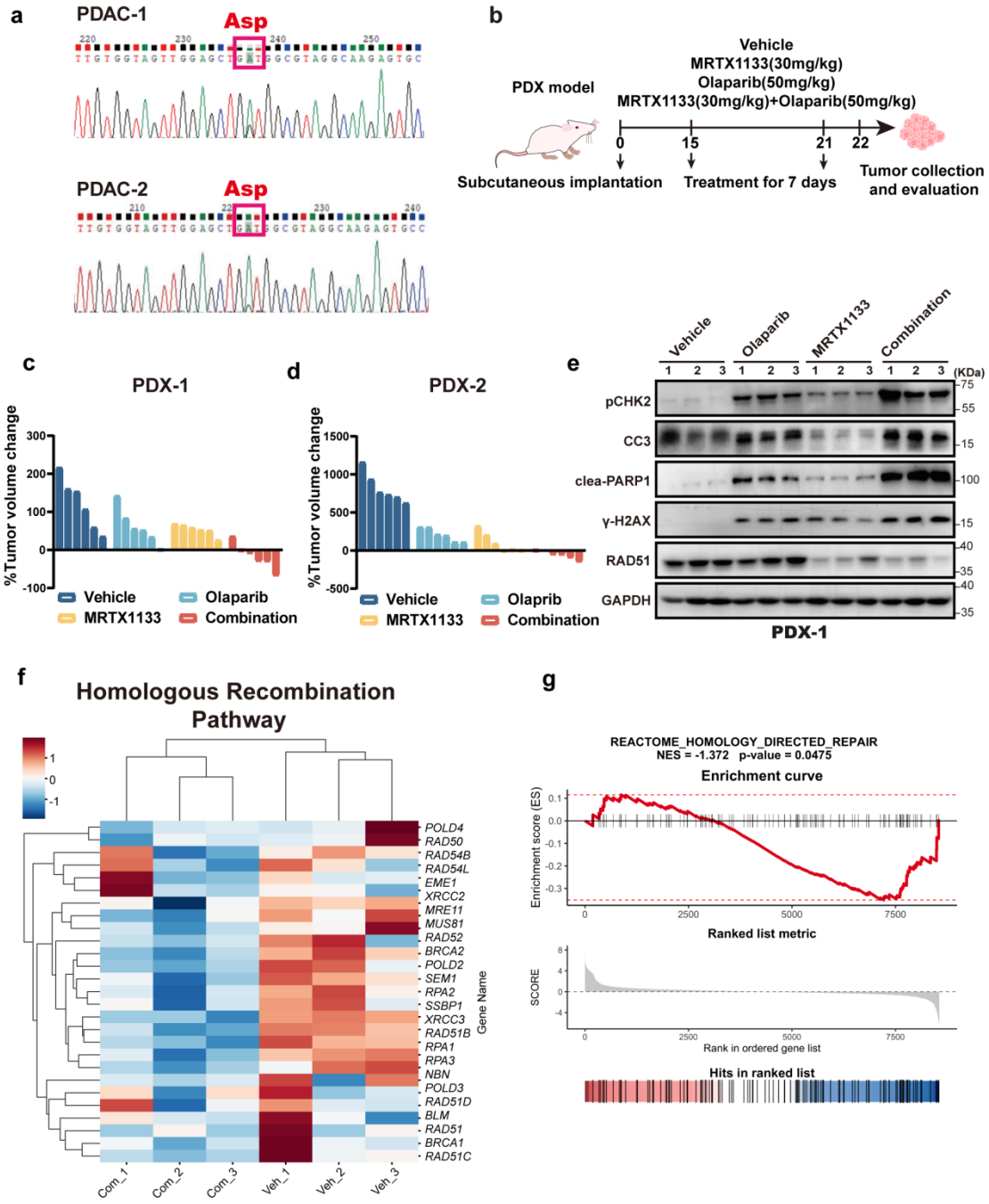


**Supplementary figure 11. Impaired HR related genes of combined treatment in KRAS$^{G12D}$ PDAC patient derived xenograft.**

**a** Sanger sequencing chromatograms confirming the presence of the KRAS$^{G12D}$ (GGT>GAT) mutation in the two PDX models used.

**b** Schematic of experiments with PDX models. Treatment (vehicle, Olaparib [50 mg/kg], MRTX1133 [30 mg/kg], or combination)was administered daily for 7 days, starting once tumors reached a measurable size (80~120 mm$^3$, day15-day21). Tumor

burden was assessed at the end of treatment (day 22) to capture early therapeutic effects.

**c-d** Waterfall plots showing the percent change in tumor volume for each individual mouse in the PDX-1 (**c**) and PDX-2 (**d**) models at the experimental endpoint. Each bar represents one mouse.

**e** Western blots showing indicated protein changes in tumor tissues after treatment in PDX-1 xenografts. pCHK2: phospho-Checkpoint kinase 2; CC3: cleaved-caspase 3; c-PARP1: cleaved-PARP1.

**f** Heatmap of HR-related genes of PDX-1. Heatmap depicting the differential expression of the indicated genes that are involved in HR signaling between combined therapy and control groups. Com: Combination therapy, Veh: vehicle (n=3 mice per group).

**g** Gene Set Enrichment Analysis (GSEA) reveals significant downregulation of the Homology Directed Repair pathway under combination treatment. GSEA plot for the "REACTOME_HOMOLOGY_DIRECTED_REPAIR" gene set. Genes were pre-ranked based on their differential expression between combination treatment and vehicle treatment, from the most upregulated (left) to the most downregulated (right). The plot demonstrates that genes within this pathway are significantly enriched among the downregulated genes, as indicated by a negative Normalized Enrichment Score (NES = -1.372) and a nominal p-value of 0.0475.

Source data are provided as a Source Data file.

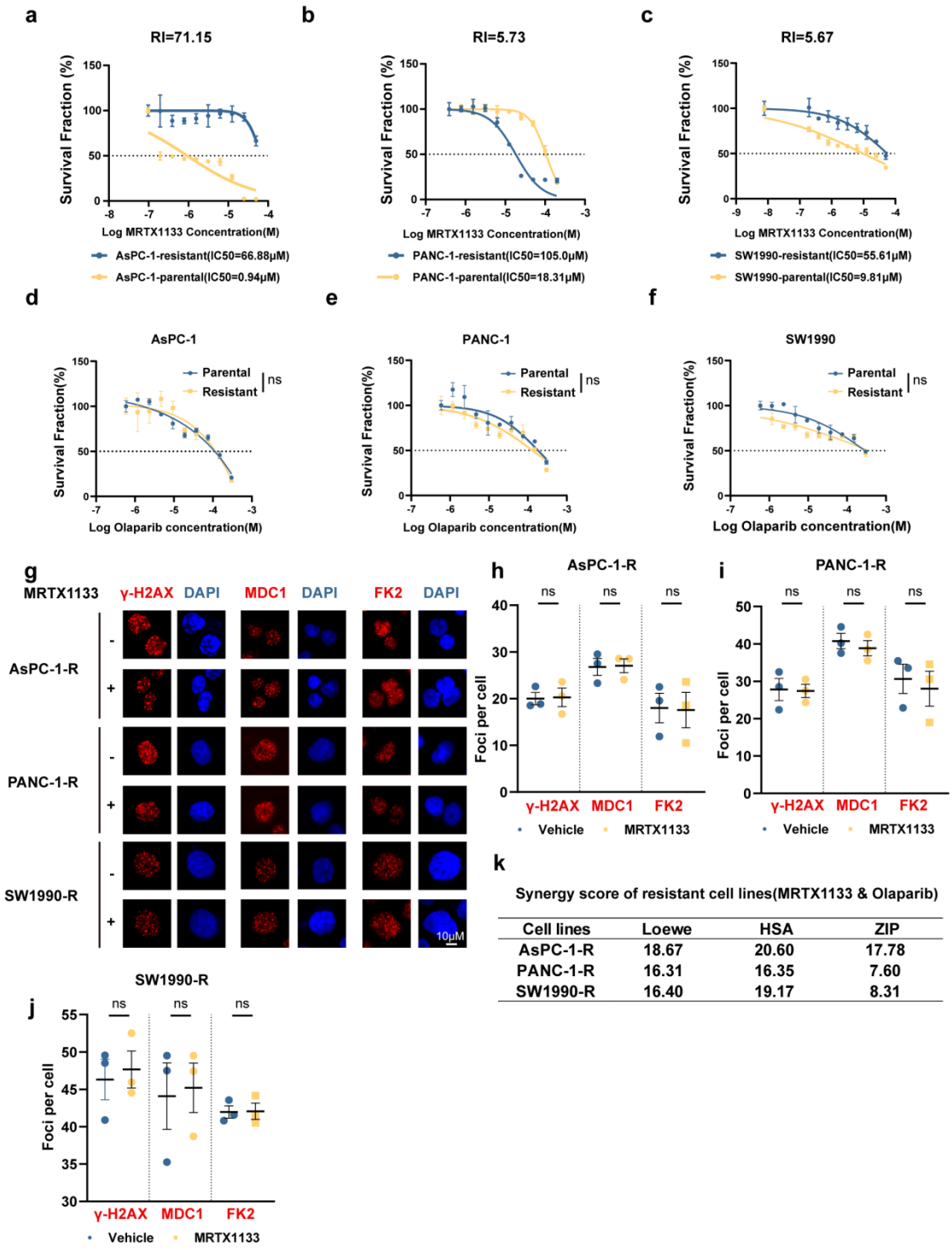


| Cell lines | Loewe | HSA | ZIP |
|---|---|---|---|
| AsPC-1-R | 18.67 | 20.60 | 17.78 |
| PANC-1-R | 16.31 | 16.35 | 7.60 |
| SW1990-R | 16.40 | 19.17 | 8.31 |

**Supplementary figure 12. MRTX1133-resistant pancreatic cancer cells retain sensitivity to Olaparib and synergistic combination therapy.**

**a-c** Establishment and validation of MRTX1133-resistant cell lines. Dose-response curves show the increased IC50 values for MRTX1133 in resistant (-R) versus parental cell lines for AsPC-1 (**a**), PANC-1 (**b**), and SW1990 (**c**). Data are presented

as mean ± SD. The Resistance Index (RI) is the ratio of IC50 values (resistant/parental).

**d-f** MRTX1133-resistan cells do not exhibit cross-resistance to Olaparib. Dose-response curves for Olaparib in parental versus resistant AsPC-1 (**d**), PANC-1 (**e**), and SW1990 (**f**) cells show no significant difference in sensitivity after 72 hours of treatment. Data are presented as mean ± SD, and statistical significance between curves was assessed by two-way ANOVA.

**g-j** Immunofluorescence assay for DNA damage marker in MRTX1133-resistant $KRAS^{G12D}$ PDAC cell lines. Representative micrographs (**g**) and quantification data for γ-H2AX, MDC1 and FK2 in AsPC-1-R (**h**), PANC-1-R (**i**), and SW1990-R (**j**) cell lines following MRTX1133 treatment(50nM). Data are presented as mean ± SEM of n=3 biologically independent experiments. Statistical significance was determined by the two-tailed unpaired t-test. Ns, no significant. The scale bar indicates 10 μm.

**k** Synergy score of Olaparib combined with MTRX1133 in resistant cell lines. Synergy score was analyzed using HSA, Loewe and ZIP models and listed in the table.

Source data are provided as a Source Data file.

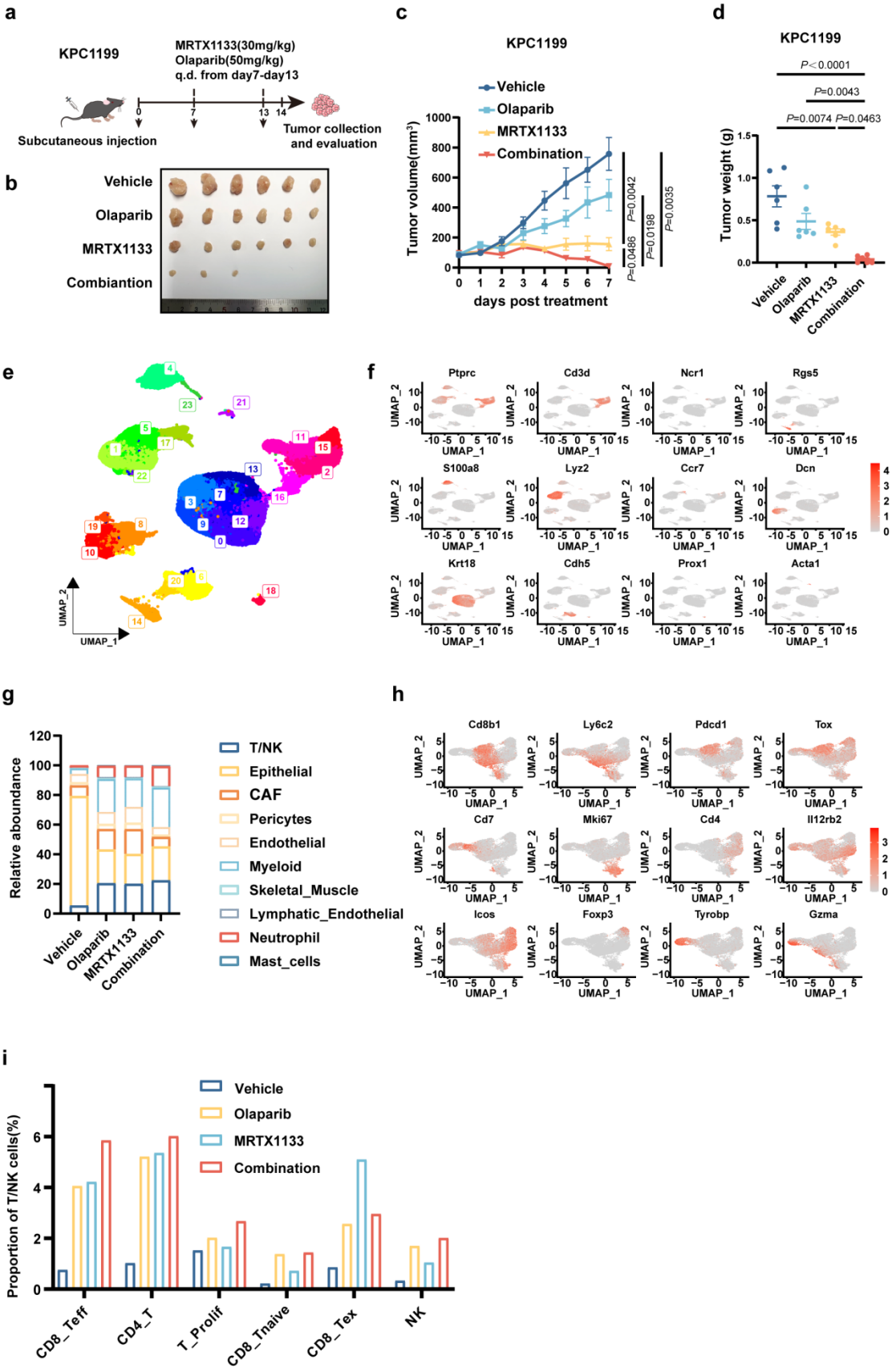


**Supplementary figure 13. Single-cell RNA sequencing (scRNA-seq) analysis**

**shows that MRTX1133 combined with Olaparib treatment modulates the tumor microenvironment in vivo.**

**a** A schematic treatment plan for immunocompetent C57BL/6J mice bearing KPC1199 tumors. Mice were subcutaneously implanted with $2 \times 10^6$ KPC1199 cells and treated with a control vehicle, inhibitors (Olaparib 50 mg/kg; qd, MRTX1133 30 mg/kg), or combined therapy, respectively.

**b** Represent image of tumors of KPC1199.

**c-d** The growth of subcutaneous KPC1199 tumors. Image of tumors was accessed at the endpoint. Tumor volume for different treatment groups was measured and the tumor growth curve was plotted (**c**). Data are presented as mean ± SEM. Statistical significance at the endpoint was assessed using two-way ANOVA.The weight of KPC1199 tumors was measured at the endpoint (**d**).Data are presented as a scatter plot where each dot represents an individual mouse (n=6), with bars indicating the mean ± SEM. Statistical significance was determined by one-way ANOVA test.

**e** Uniform Manifold Approximation and Projection (UMAP) plot of all cells analyzed by scRNA-seq, showing 24 distinct clusters identified across all treatment groups.

**f** UMAP feature plots showing the expression of canonical marker genes used to identify major cell lineages within the tumor microenvironment.

**g** Stacked bar chart showing the relative abundance of major cell populations across the four treatment groups, as determined from the scRNA-seq data.

**h** UMAP feature plots displaying the expression of key marker genes used to further define T-cell and NK-cell subsets.

**i** Bar chart showing the proportion of specific T-cell and NK-cell subsets as a percentage of the total T/NK cell population in each treatment group. (Teff: effector T-cell; T_Prolif: proliferating T-cell; Tnaive: naive T-cell; Tex: exhausted T-cell).

Ns, no significant. Source data are provided as a Source Data file.

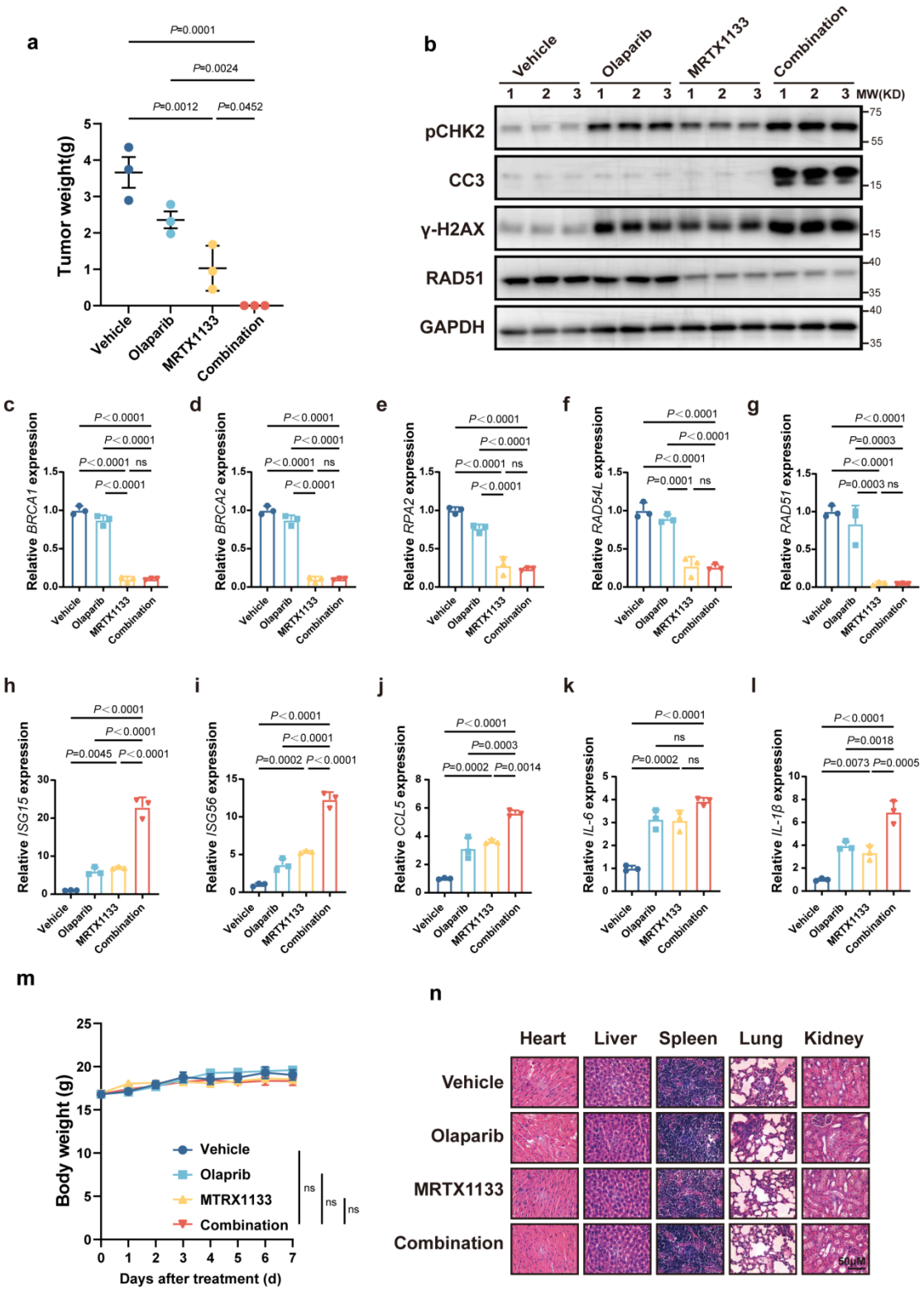


**Supplementary figure 14. Enhanced immune activation and rational safety of combined treatment in orthotopic model.**

**a** Endpoint tumor weights from mice bearing orthotopic KPC1199 tumors after 7 days of treatment. Data are presented as a scatter plot where each dot represents an

individual mouse (n=3 per group), with bars indicating mean ± SEM. Statistical significance was determined by one-way ANOVA with Tukey' s multiple comparisons test.

**b** Western blots showing indicated protein changes in tumor tissues collected at endpoint of survival cohort. pCHK2: phosphorous-Checkpoint kinase 2; CC3: cleaved-caspase 3.

**c-g** RNA level of HR-related genes among all subgroups in orthotopic tumor of survival cohort. Relative mRNA expression in orthotopic tumors (n=3 per group) was measured by RT-qPCR. Data are presented as mean ± SEM. Statistical significance was determined by one-way ANOVA test.

**h-l** Quantitative PCR of interferon stimulated and cytokine genes among four groups of survival cohort. Upregulation of interferon related genes in monotherapy and combined therapy was confirmed.

**m** Body weight of the orthotopic models during treatment of survival cohort. Body weight of mice during the treatment period, showing no significant weight loss in any group (n=10 per group). Data are presented as mean ± SEM. Statistical significance at the endpoint was determined by two-way ANOVA.

**n** Representative images of HE staining for multiple internal organs are shown with treatment indicated in C57BL6/J bearing pancreatic tumors orthotopically.

Ns, no significant. Source data are provided as a Source Data file.

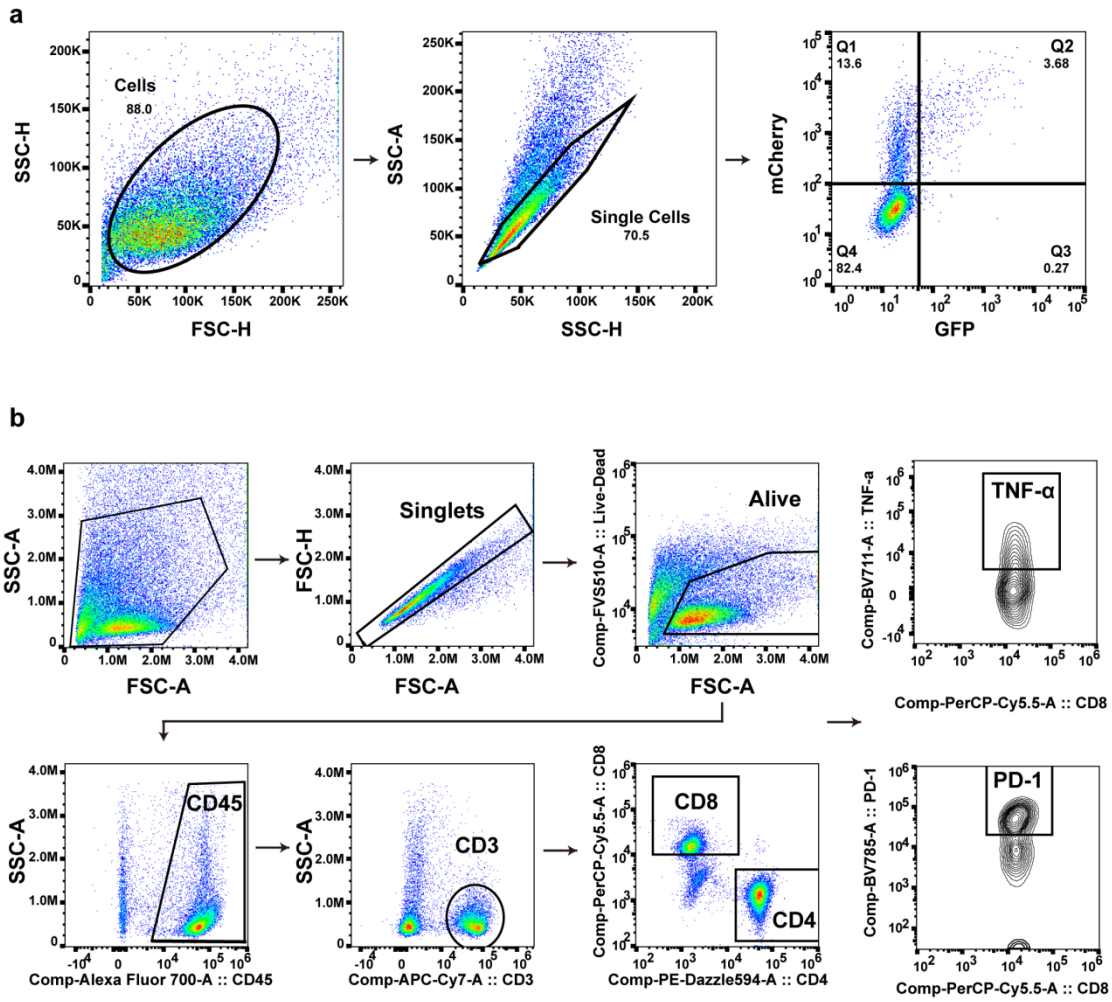


**Supplementary figure 15. Gate strategy of flow cytometry**

**a** Gating strategy for HR reporter assays, HR repair efficiency = Q2/(Q1 + Q2).

**b** The representative FACS gating strategies for analyzing tumor-infiltrating lymphocytes. Cells were first gated by FSC-A and FSC-H to eliminate non-singlet cells and gated by SSC-A/comp-FVS510-A to eliminate dead cells. This gating strategy is suitable for analyzing all tumor-infiltrating leukocytes.

Supp.Fig.3a

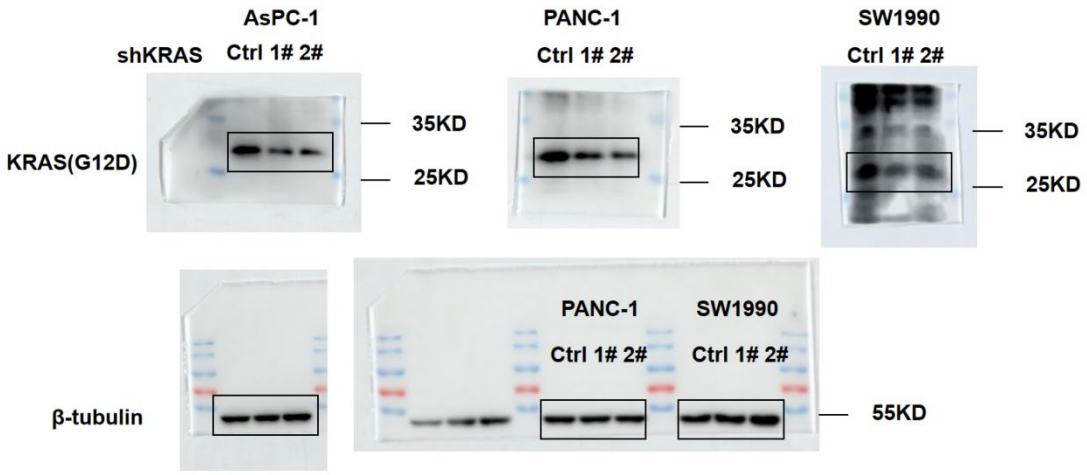
AsPC-1
PANC-1
SW1990
shKRAS
Ctrl 1# 2#
Ctrl 1# 2#
Ctrl 1# 2#
KRAS(G12D)
35KD
25KD
35KD
25KD
35KD
25KD
β-tubulin
PANC-1
SW1990
Ctrl 1# 2#
Ctrl 1# 2#
55KD

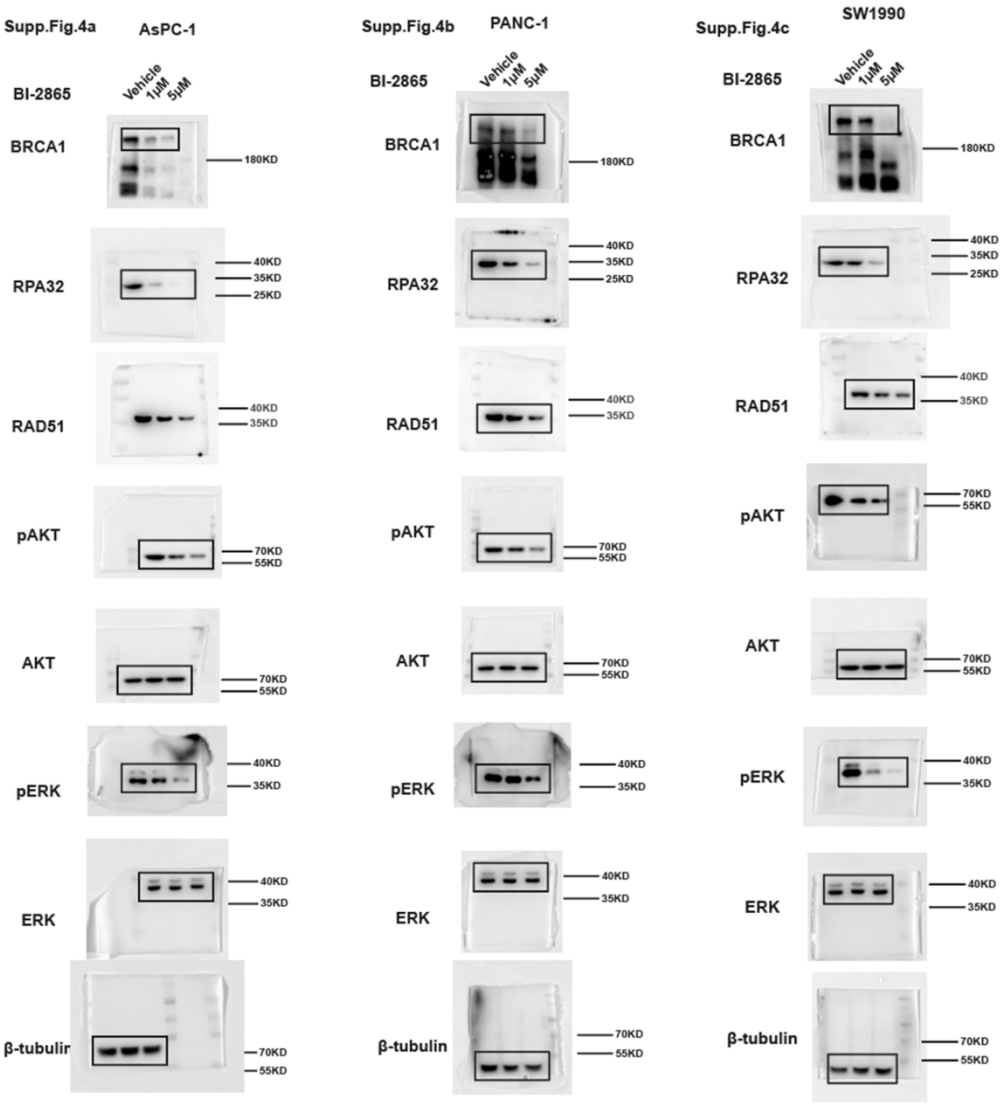
Supp.Fig.4a
AsPC-1
BI-2865
Vehicle
1μM
5μM
BRCA1
180KD
RPA32
40KD
35KD
25KD
RAD51
40KD
35KD
pAKT
70KD
55KD
AKT
70KD
55KD
pERK
40KD
35KD
ERK
40KD
35KD
β-tubulin
70KD
55KD
Supp.Fig.4b
PANC-1
BI-2865
Vehicle
1μM
5μM
BRCA1
180KD
RPA32
40KD
35KD
25KD
RAD51
40KD
35KD
pAKT
70KD
55KD
AKT
70KD
55KD
pERK
40KD
35KD
ERK
40KD
35KD
β-tubulin
70KD
55KD
Supp.Fig.4c
SW1990
BI-2865
Vehicle
1μM
5μM
BRCA1
180KD
RPA32
40KD
35KD
25KD
RAD51
40KD
35KD
pAKT
70KD
55KD
AKT
70KD
55KD
pERK
40KD
35KD
ERK
40KD
35KD
β-tubulin
70KD
55KD

Supp.Fig.4n

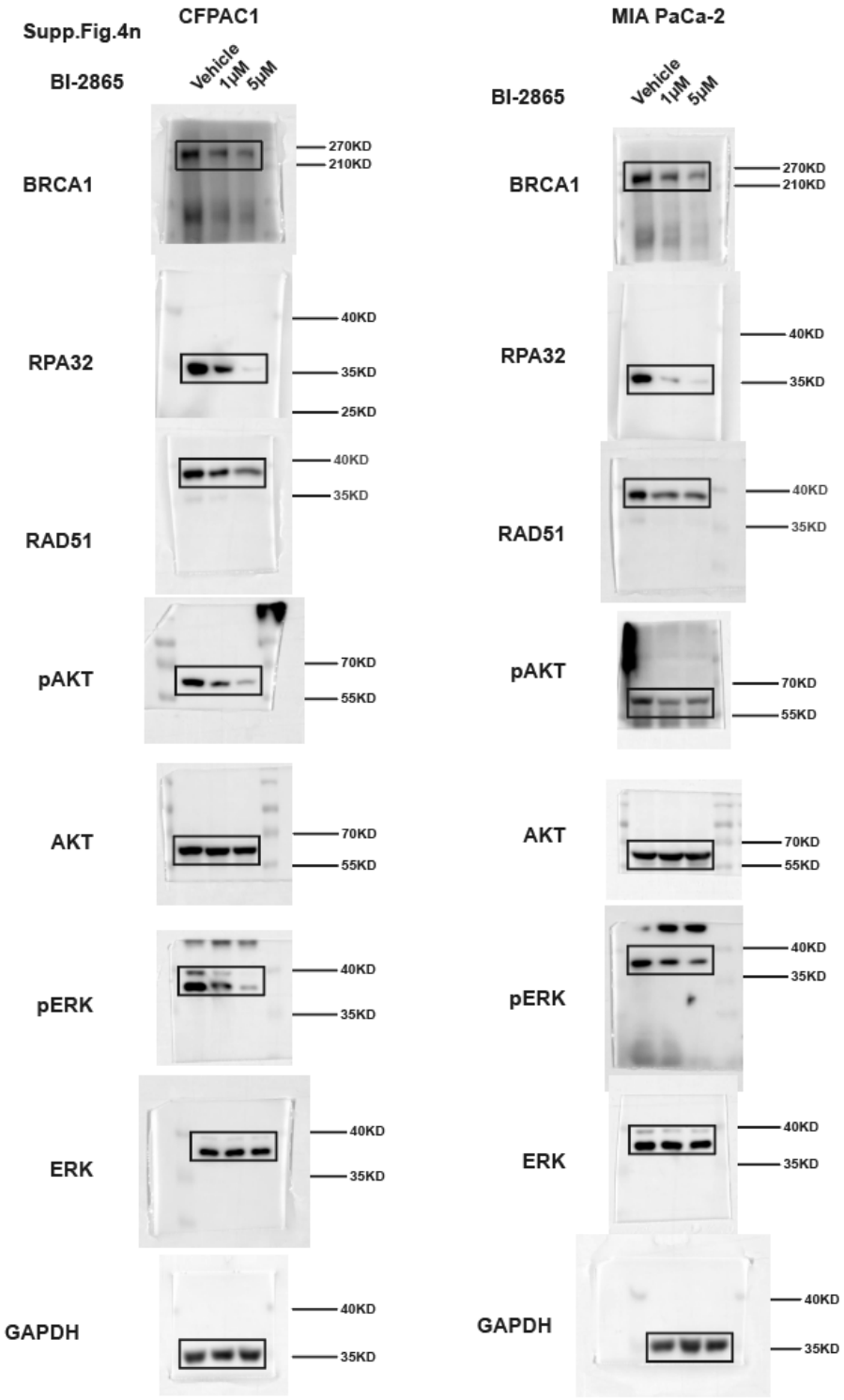
CFPAC1
MIA PaCa-2
BI-2865
Vehicle
1μM
5μM
BRCA1
270KD
210KD
RPA32
40KD
35KD
25KD
RAD51
pAKT
70KD
55KD
AKT
pERK
ERK
GAPDH

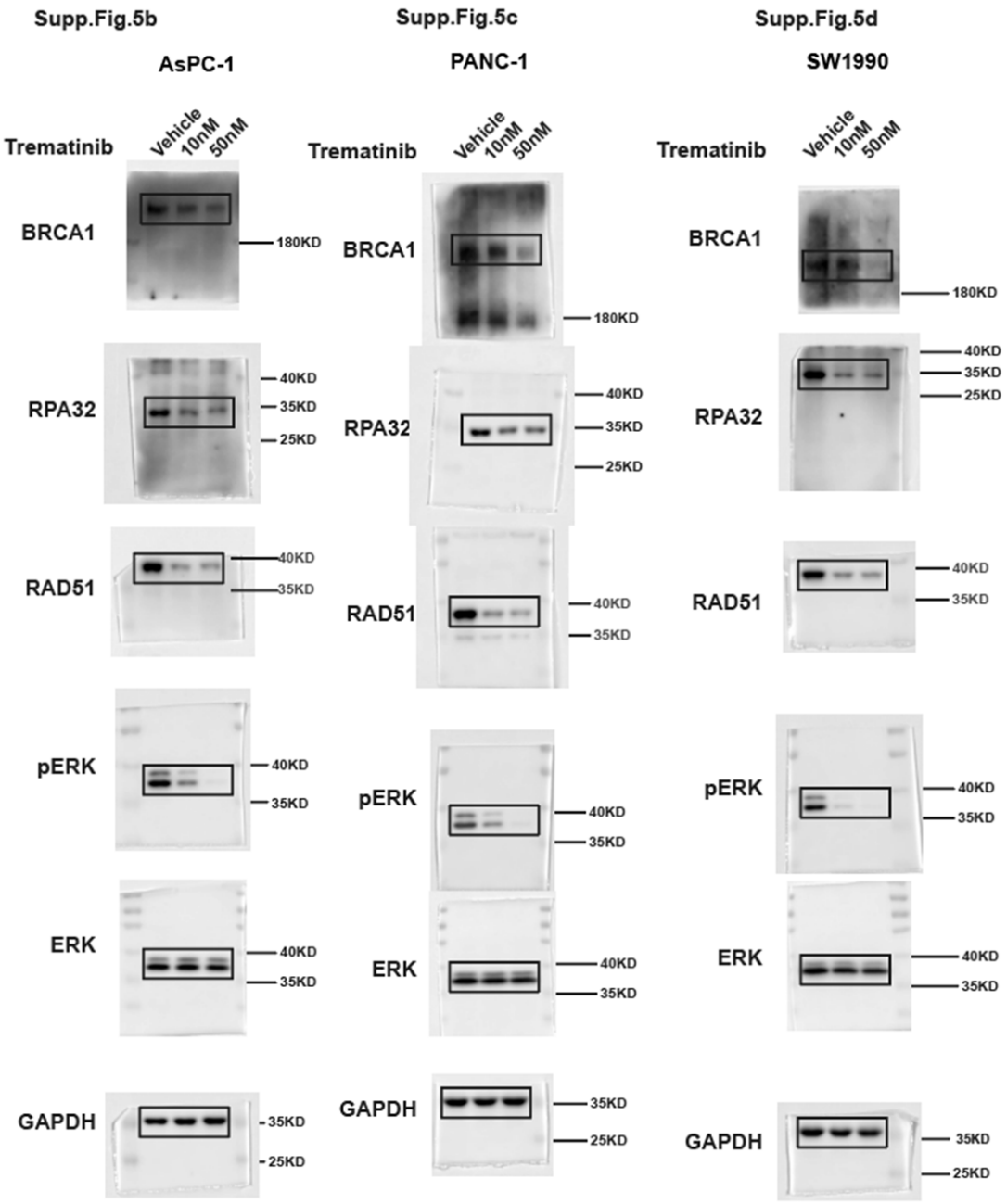
Supp.Fig.5b
AsPC-1
Trematinib
Vehicle
10nM
50nM
BRCA1
180KD
RPA32
40KD
35KD
25KD
RAD51
40KD
35KD
pERK
40KD
35KD
ERK
40KD
35KD
GAPDH
35KD
25KD
Supp.Fig.5c
PANC-1
Trematinib
Vehicle
10nM
50nM
BRCA1
180KD
RPA32
40KD
35KD
25KD
RAD51
40KD
35KD
pERK
40KD
35KD
ERK
40KD
35KD
GAPDH
35KD
25KD
Supp.Fig.5d
SW1990
Trematinib
Vehicle
10nM
50nM
BRCA1
180KD
RPA32
40KD
35KD
25KD
RAD51
40KD
35KD
pERK
40KD
35KD
ERK
40KD
35KD
GAPDH
35KD
25KD

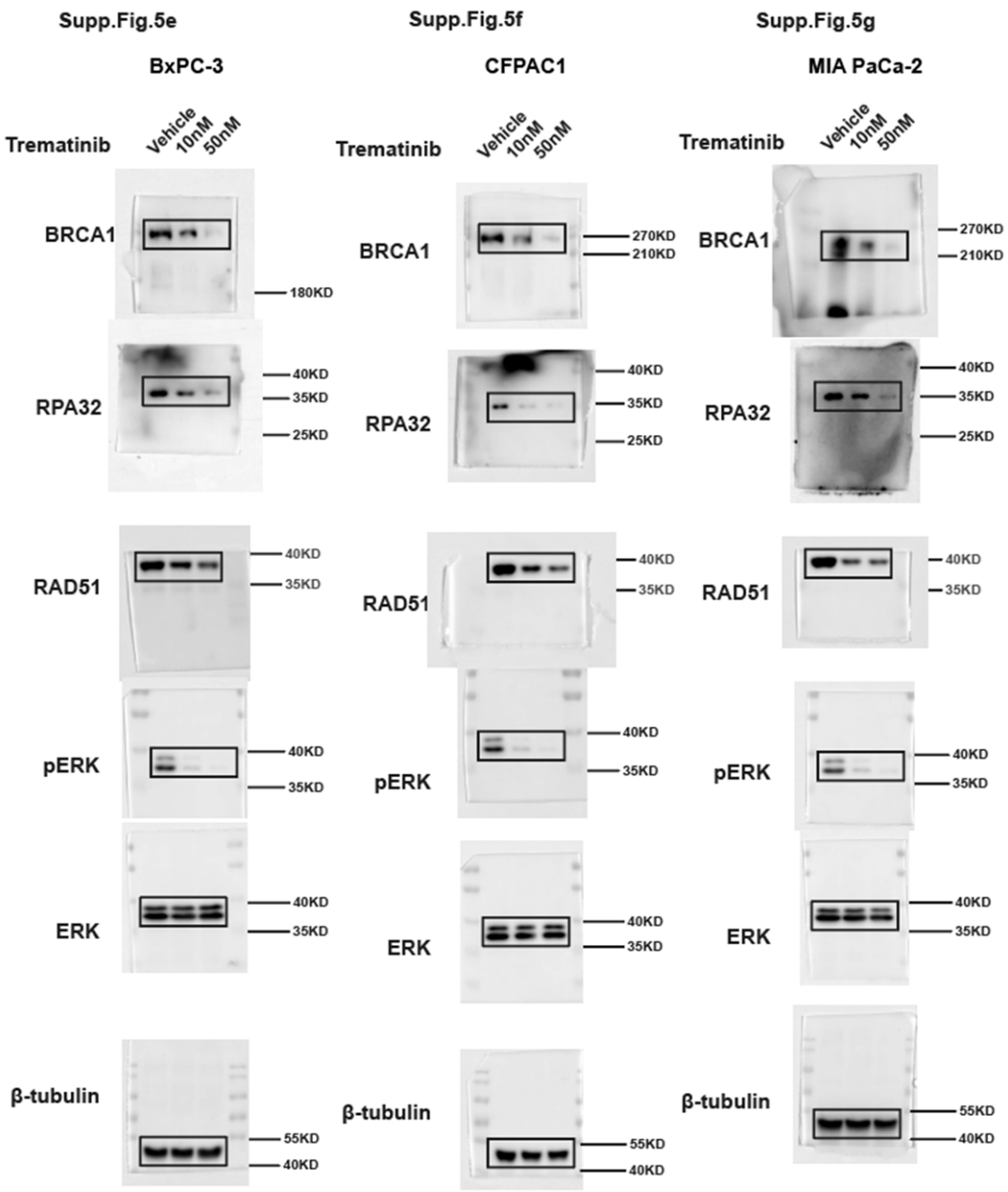
Supp.Fig.5e
BxPC-3
Trematinib
Vehicle
10nM
50nM
BRCA1
180KD
RPA32
40KD
35KD
25KD
RAD51
40KD
35KD
pERK
40KD
35KD
ERK
40KD
35KD
β-tubulin
55KD
40KD
Supp.Fig.5f
CFPAC1
Trematinib
Vehicle
10nM
50nM
BRCA1
270KD
210KD
RPA32
40KD
35KD
25KD
RAD51
40KD
35KD
pERK
40KD
35KD
ERK
40KD
35KD
β-tubulin
55KD
40KD
Supp.Fig.5g
MIA PaCa-2
Trematinib
Vehicle
10nM
50nM
BRCA1
270KD
210KD
RPA32
40KD
35KD
25KD
RAD51
40KD
35KD
pERK
40KD
35KD
ERK
40KD
35KD
β-tubulin
55KD
40KD

Supp.Fig.7c

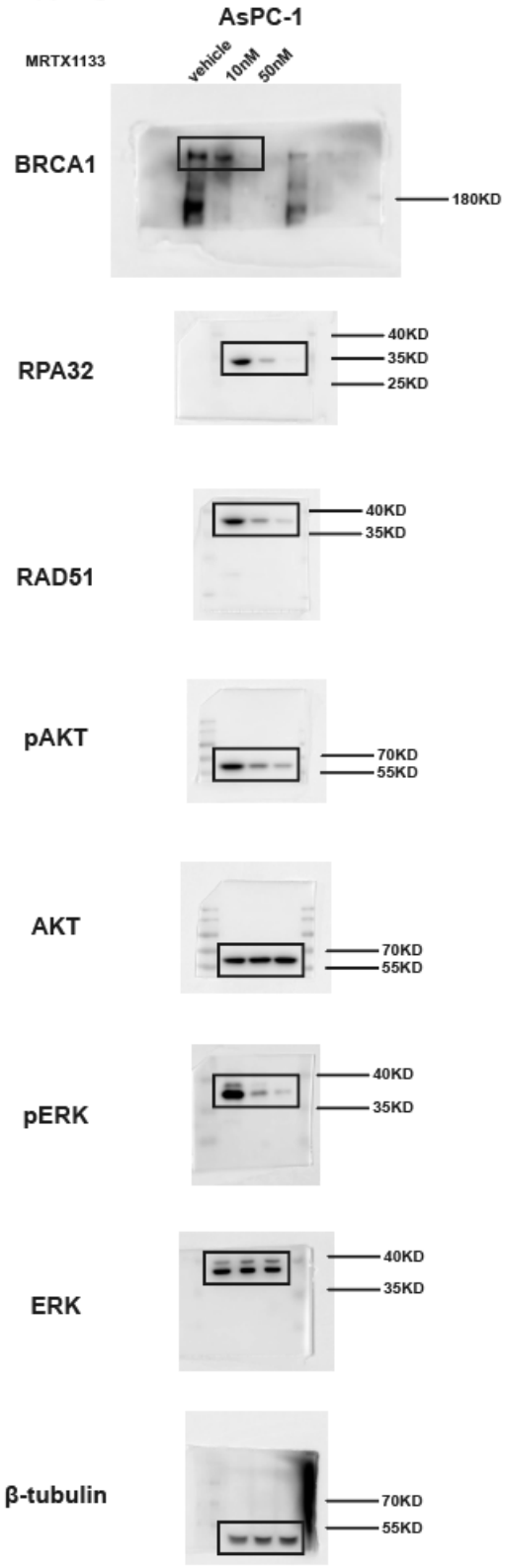


Supp.Fig.7d

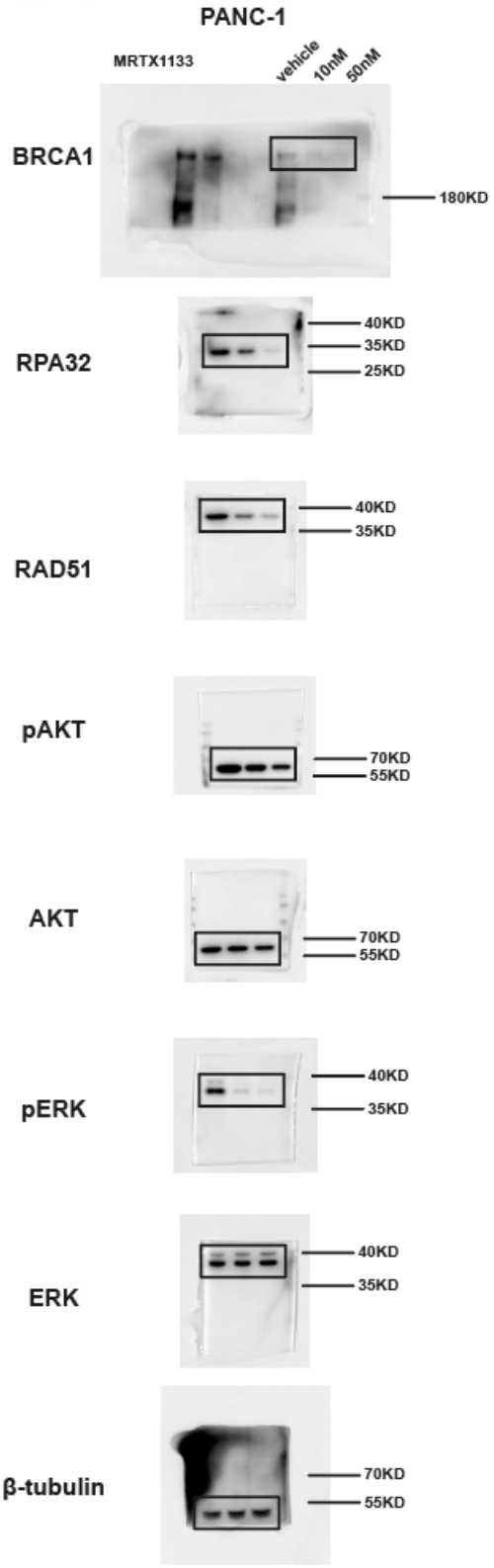

Supp.Fig.7e

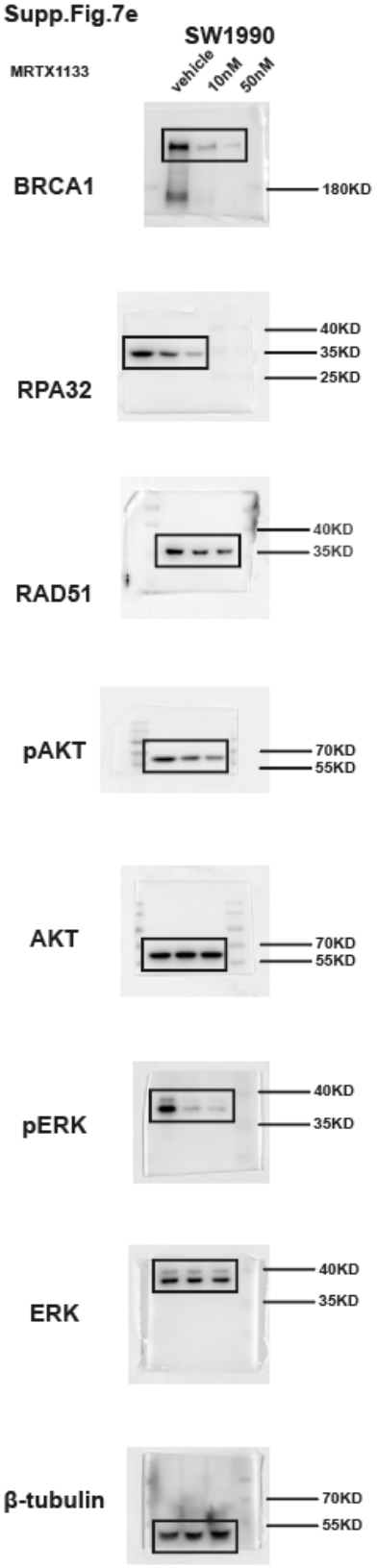


Supp.Fig.7f

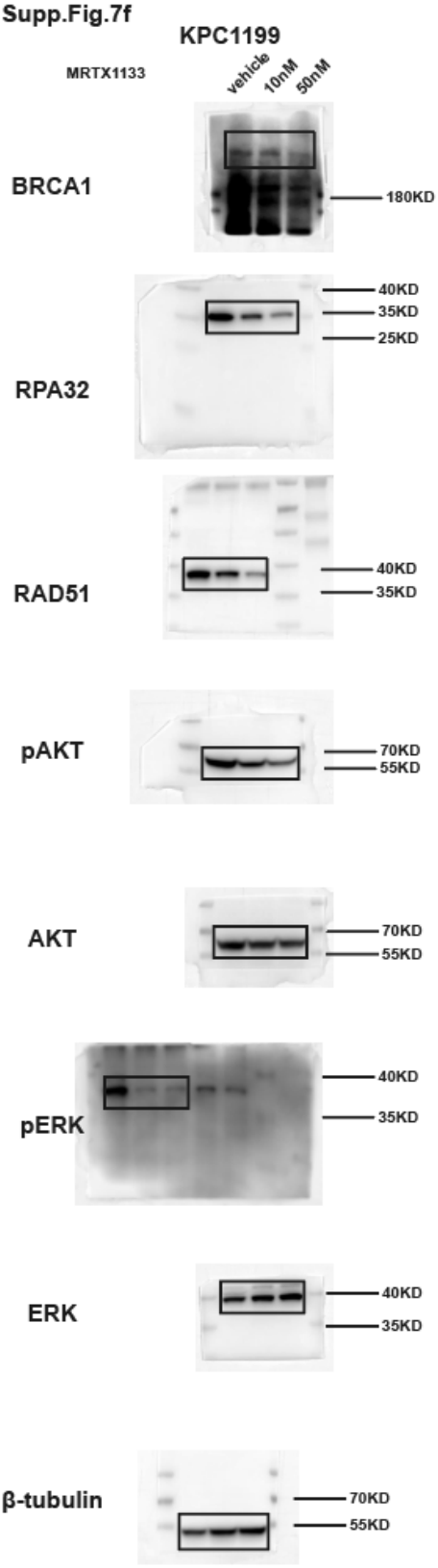

Supp.Fig.8a

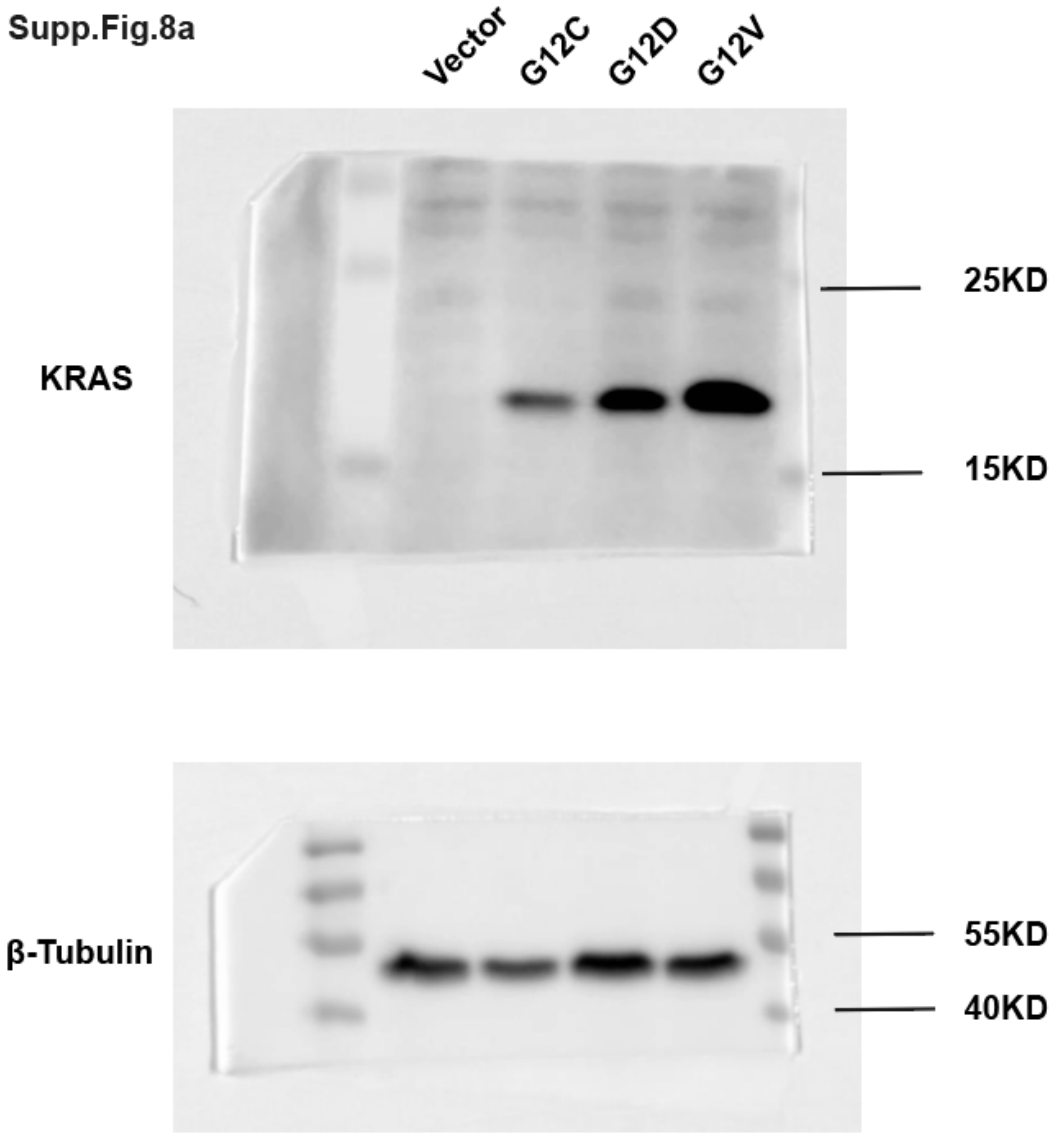

Supp.Fig.8e CFPAC1(synchronized)

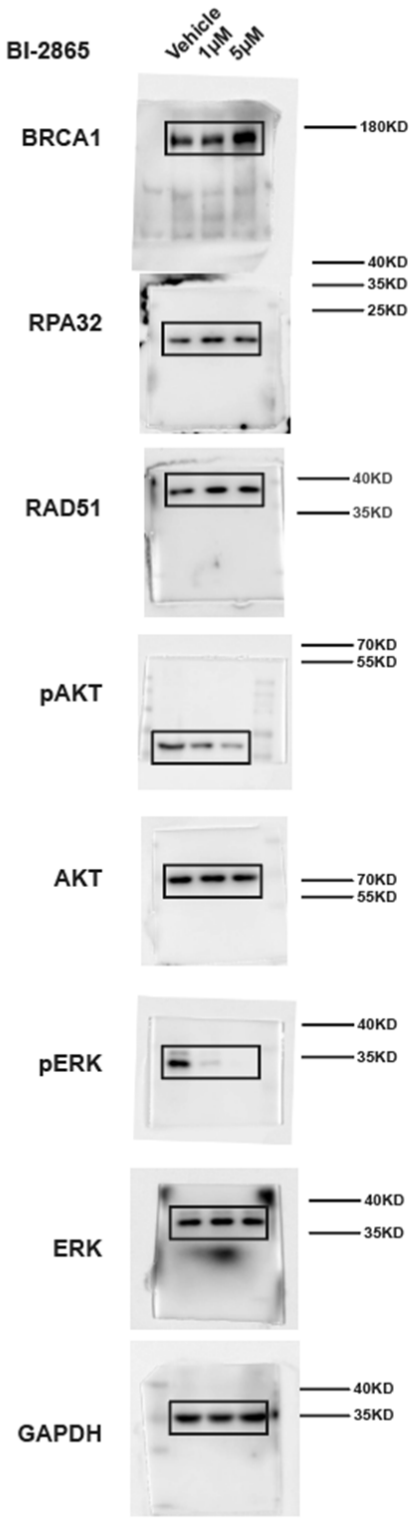


Supp.Fig.8f MIA PaCa-2(synchronized)

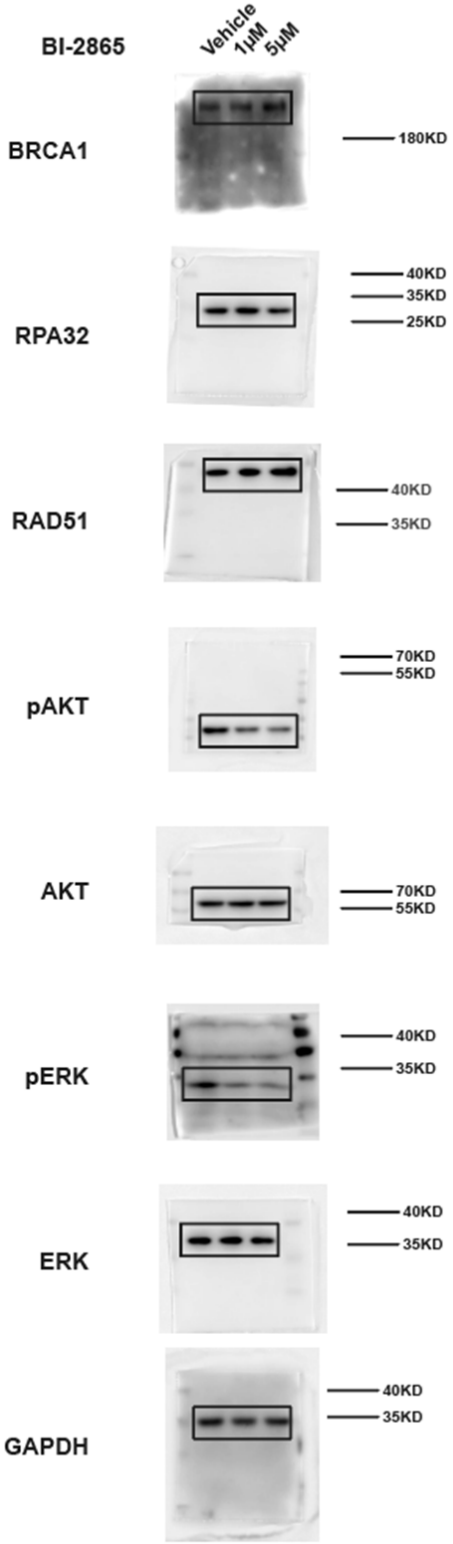

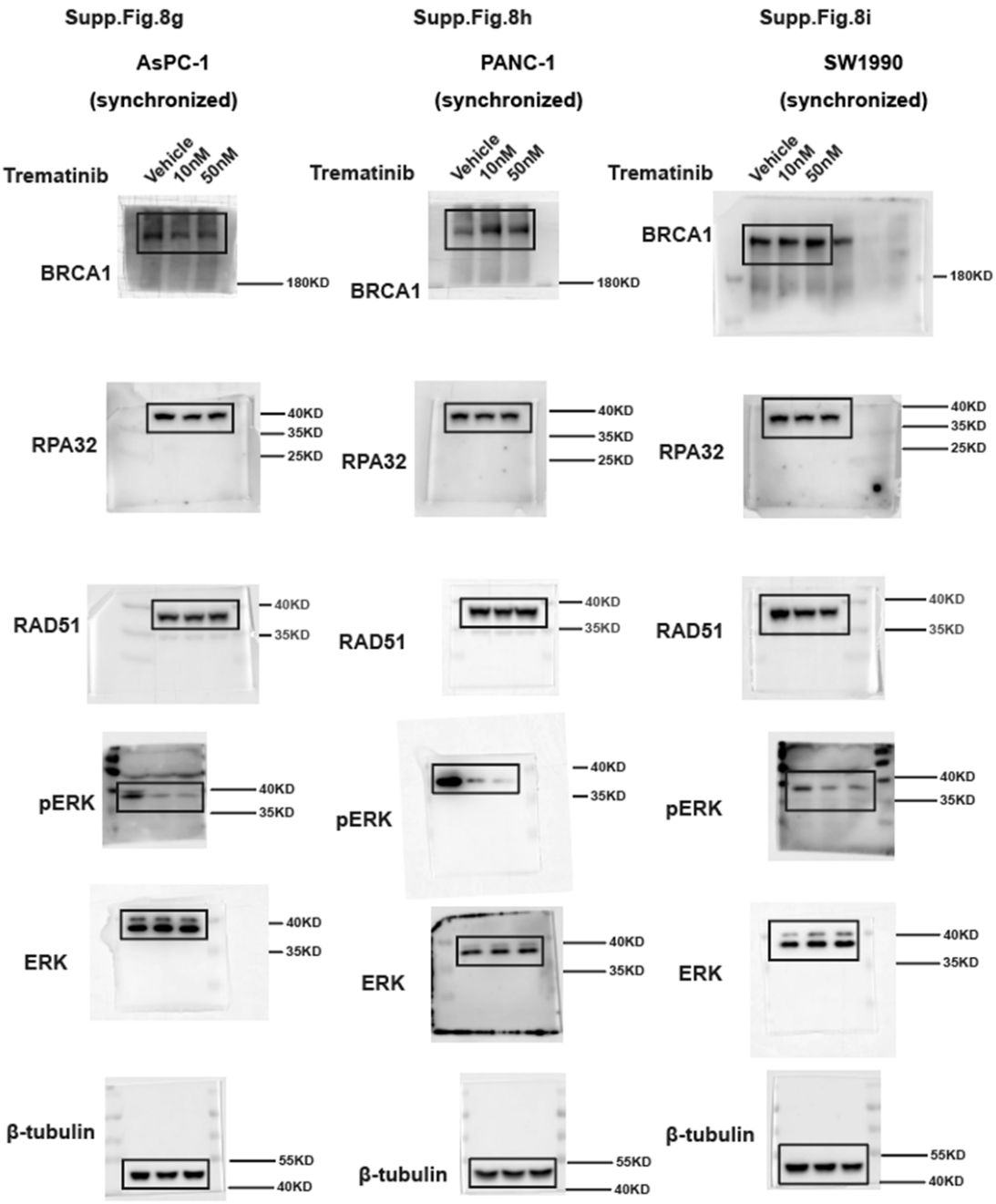
Supp.Fig.8g
AsPC-1
(synchronized)
Supp.Fig.8h
PANC-1
(synchronized)
Supp.Fig.8i
SW1990
(synchronized)
Trematinib
Vehicle
10nM
50nM
BRCA1
180KD
RPA32
40KD
35KD
25KD
RAD51
pERK
ERK
β-tubulin
55KD

Supp.Fig.8j

BxPC-3

(synchronized)

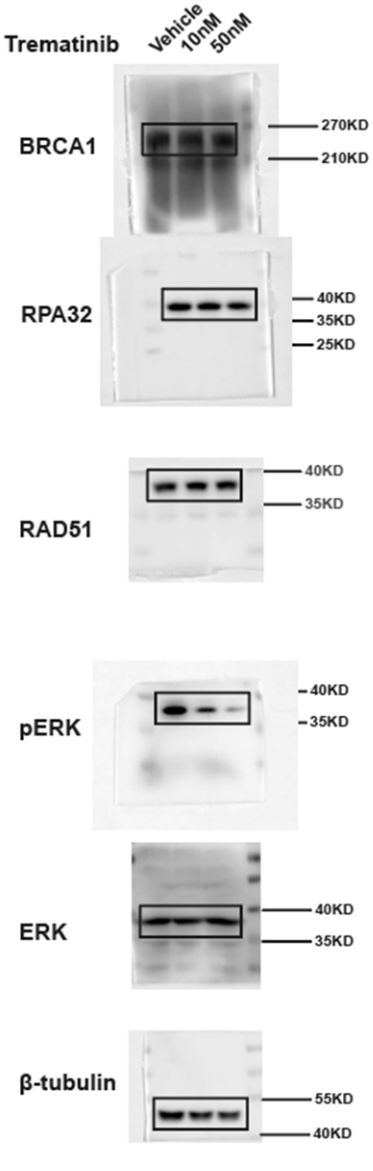


Supp.Fig.8k

CFPAC1

(synchronized)

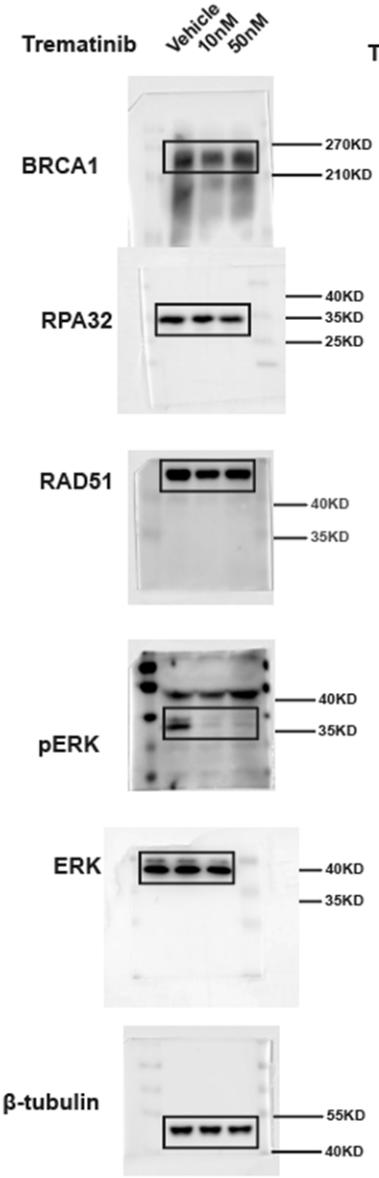


Supp.Fig.8l

MIA PaCa-2

(synchronized)

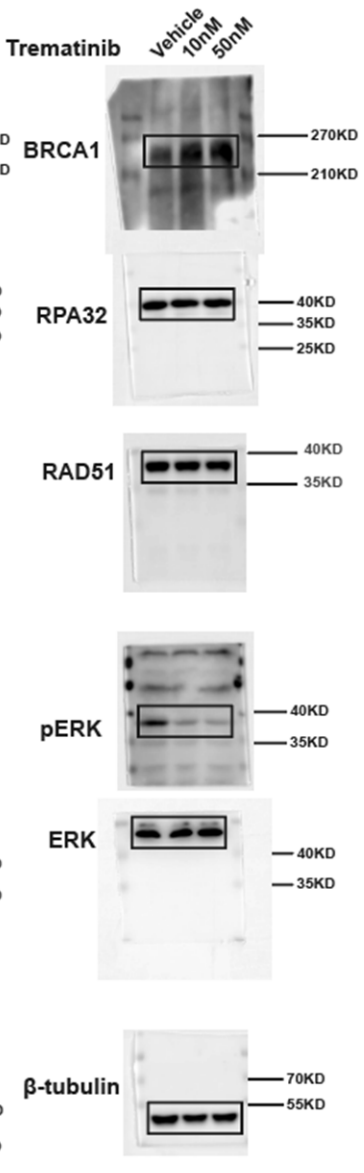

Supp.Fig.10c

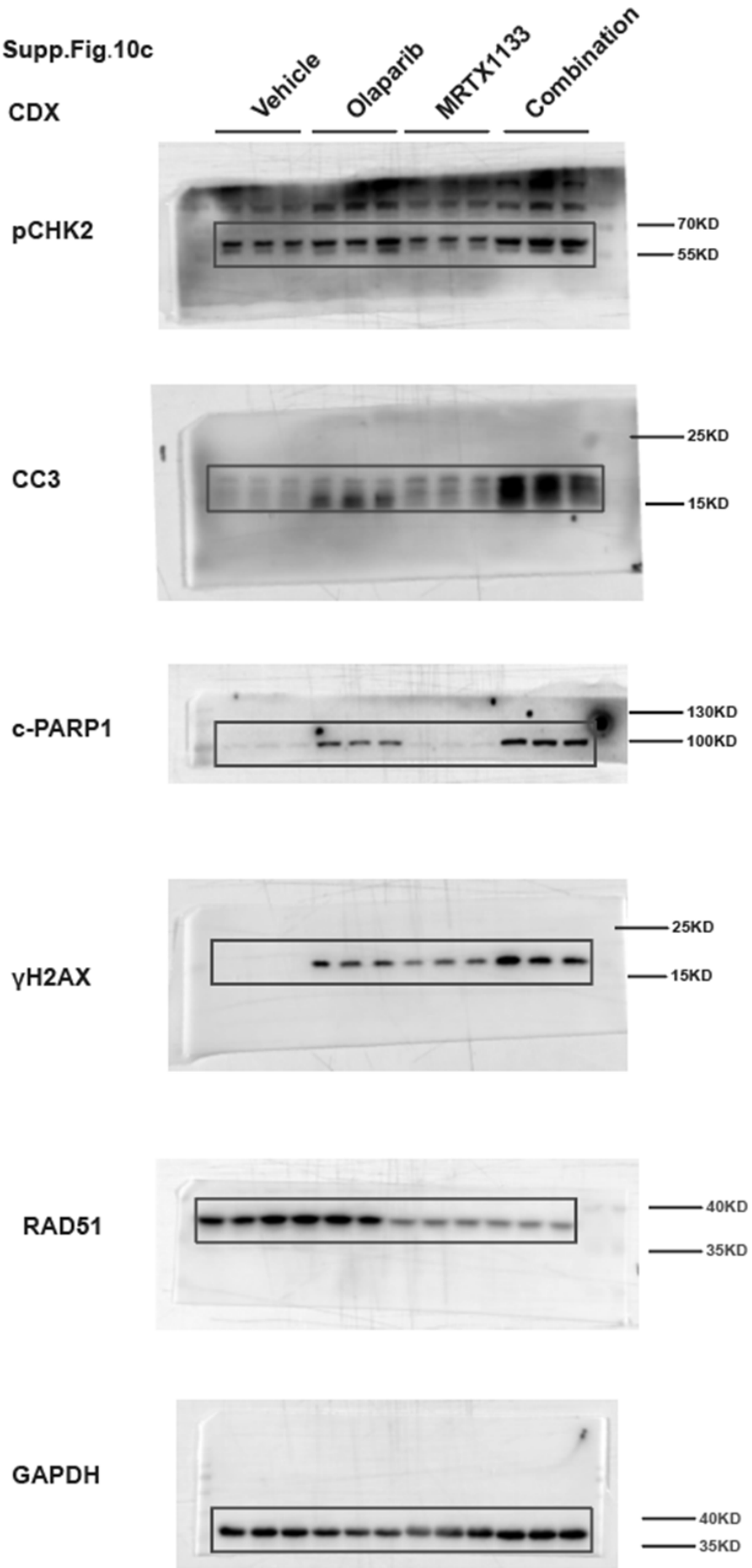
CDX
Vehicle
Olaparib
MRTX1133
Combination
pCHK2
70KD
55KD
CC3
25KD
15KD
c-PARP1
130KD
100KD
γH2AX
25KD
15KD
RAD51
40KD
35KD
GAPDH
40KD
35KD

Supp.Fig.11e

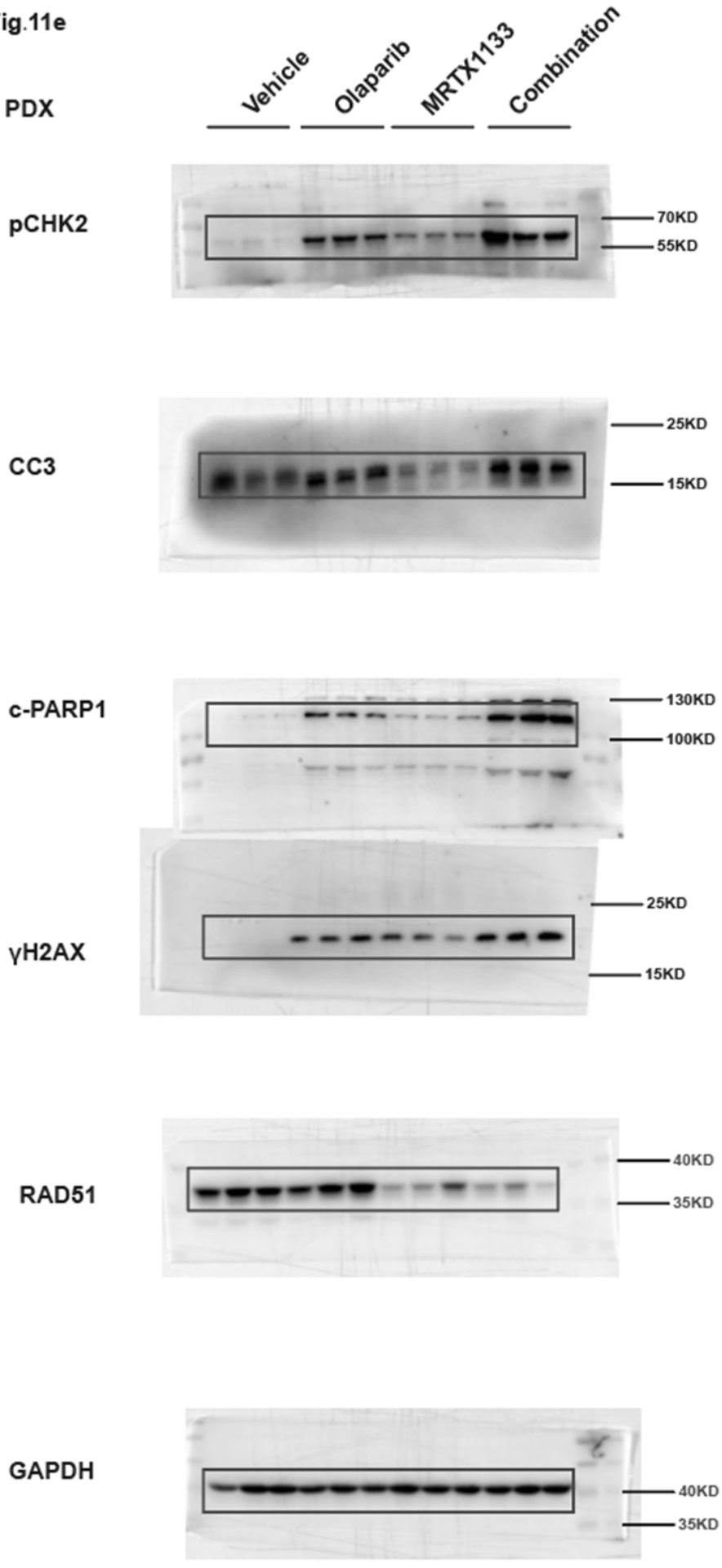
PDX
Vehicle
Olaparib
MRTX1133
Combination
pCHK2
70KD
55KD
CC3
25KD
15KD
c-PARP1
130KD
100KD
γH2AX
25KD
15KD
RAD51
40KD
35KD
GAPDH
40KD
35KD

Supp.Fig.14b

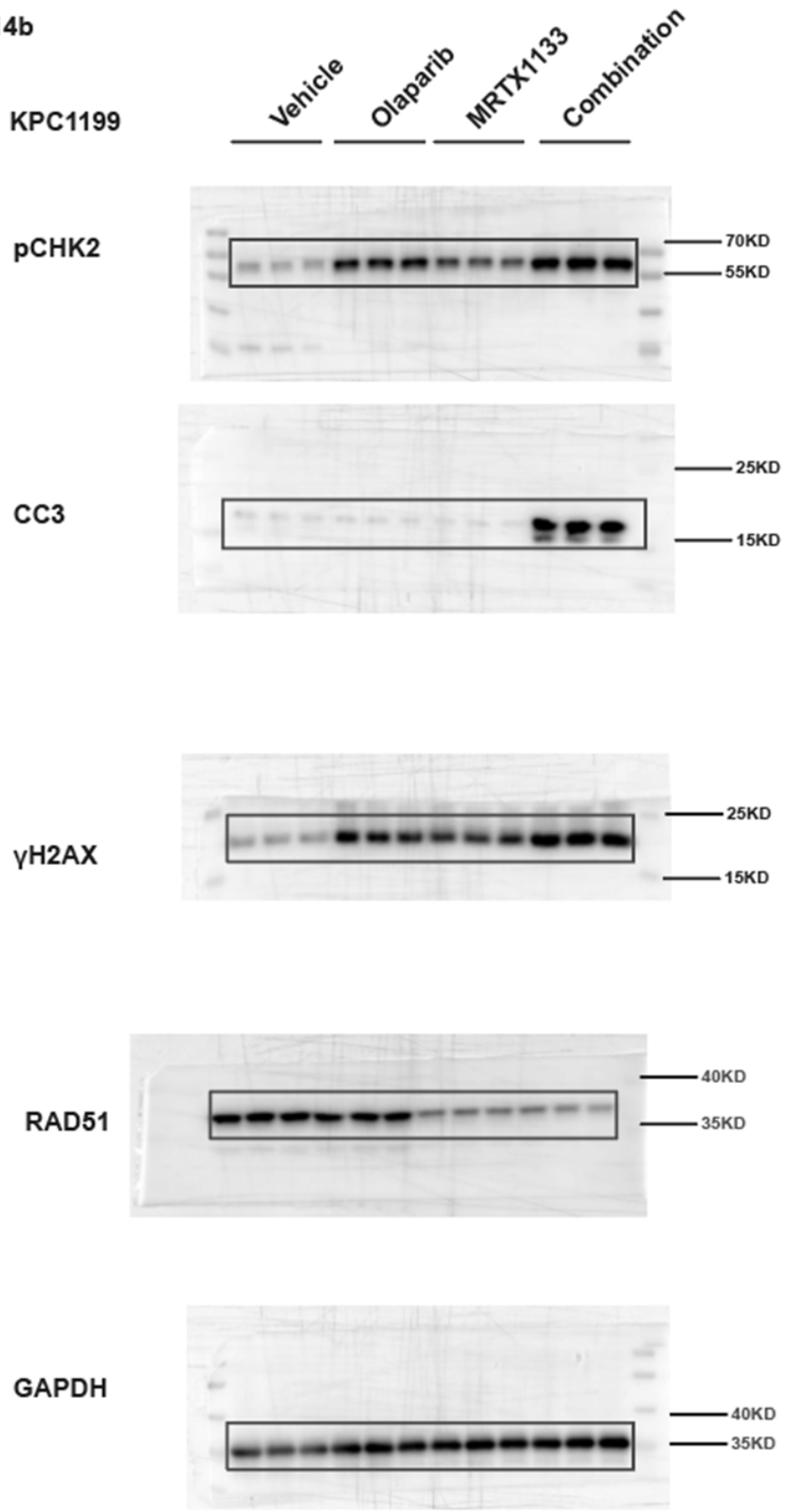
KPC1199
Vehicle
Olaparib
MRTX1133
Combination
pCHK2
70KD
55KD
CC3
25KD
15KD
γH2AX
25KD
15KD
RAD51
40KD
35KD
GAPDH
40KD
35KD